Master's Thesis

The metabolic responses to electrical pulse-induced contractions in C2C12 myotubes are greater in high glucose medium

Sakari Mäntyselkä

University of Jyväskylä

Department of Biological and Environmental Science

Cell and Molecular Biology

15th April 2021

UNIVERSITY OF JYVÄSKYLÄ, Faculty of Mathematics and Science
Department of Biological and Environmental Science
Cell and Molecular Biology

Sakari Mäntyselkä:	The metabolic responses to electrical pulse-induced contractions in C2C12 myotubes are greater in high glucose medium
MSc thesis:	42 p., 6 appendices (6 p.)
Supervisors:	Associate Professor Juha Hulmi and Professor Perttu Permi
Reviewers:	Professor Jari Ylänne and University Researcher Maarit Lehti

April 2021

Keywords: ACOT9, BSCFAs, cell model, exercise model, metabolomics, skeletal muscle

Some of the mechanisms behind the favorable effects of physical activity are difficult to study *in vivo.* Electrical pulse stimulation (EPS) of the cultured myotubes has become a widely used *in vitro* model to mimic *in vivo* muscle contractions and exercise. However, its detailed effects on metabolic processes are still poorly known. The C2C12 myotubes are usually cultured in supraphysiological 25 mM glucose conditions, which can affect EPS responses. In this present study, C2C12 myotubes were electrical pulse stimulated for 24 hours in low (5.5 mM) and high (25 mM) glucose (LG and HG respectively) conditions, and both intra- and extracellular metabolites were analyzed using untargeted nuclear magnetic resonance (NMR) spectroscopy. In response to EPS, the C2C12 myotubes increased glucose consumption and secreted large amounts of lactate and acetate in both glucose conditions but especially in HG condition. In addition, the C2C12 myotubes secreted branched short-chain fatty acids (BSCFAs) and a ketone body 3-hydroxybutyrate in response to EPS, especially in HG condition. Intracellular BSCFAs and branched-chain amino acids (BCAAs) correlated highly and BSCFA content substantially decreased when myotubes were cultured in BCAA-free medium, suggesting that BSCFAs were formed through the catabolism of BCAAs and possibly by acyl-CoA thioesterase 9 (ACOT9) enzyme. The results suggest that nutrient availability is an important factor to consider in future studies. Further, the role of acetate and BSCFAs in inter-organ metabolic communication would be beneficial to study in the future.

JYVÄSKYLÄN YLIOPISTO, Matemaattis-luonnontieteellinen tiedekunta
Bio- ja ympäristötieteiden laitos
Solu- ja Molekyylibiologia

Sakari Mäntyselkä: Aineenvaihdunnalliset vasteet sähköpulsseilla indusoituihin lihassupistuksiin C2C12 myotuubeissa ovat suuremmat, kun glukoosin saatavuus on korkeampi
Pro gradu -tutkielma: 42 s., 6 liitettä (6 s.)
Työn ohjaajat: Apulaisprofessori Juha Hulmi ja professori Perttu Permi
Tarkastajat: Professori Jari Ylänne ja yliopistotutkija Maarit Lehti
Huhtikuu 2021

Hakusanat: ACOT9, BSCFAs, liikuntamalli, luurankolihas, metabolomiikka, solumalli

Osaa liikunnan terveyshyötyjen mekanismeista on vaikeaa tutkia ihmisillä tai koe-eläimillä. Viljeltyjen C2C12 myotuubien sähköpulssistimulaatiolla (EPS, engl. electrical pulse stimulation) voidaan mallintaa lihassupistuksia ja liikuntaa *in vitro* –olosuhteissa. EPS:n vaikutusta C2C12 myotuubien aineenvaihduntaan ei kuitenkaan tunneta tarkasti. Lisäksi C2C12 myotuubeja viljellään yleensä korkeassa ei-fysiologisessa 25 mM glukoosipitoisuudessa, mikä voi vaikuttaa EPS-vasteisiin. Tässä tutkimuksessa C2C12 myotuubeja sähköpulssistimuloitiin 24 tunnin ajan sekä matalan 5.5 mM (MG) että korkean 25 mM (KG) glukoosipitoisuuden olosuhteissa, ja aineenvaihduntatuotteiden konsentraatiot analysoitiin sekä soluista että elatusaineesta ydinmagneettisella resonanssispektroskopialla (NMR). EPS:n vaikutuksesta, solut käyttivät enemmän glukoosia sekä erittivät paljon laktaattia ja asetaattia molemmissa glukoosipitoisuuksissa, mutta etenkin KG-olosuhteissa. Lisäksi etenkin KG-olosuhteissa C2C12 myotuubit erittivät haaroittuneita lyhytketjuisia rasvahappoja (BSCFA) ja ketoaine 3-hydroksibutyraattia. Edelleen havaittiin, että BSCFA:t korreloivat vahvasti haaraketjuisten aminohappojen (BCAA) kanssa myotuubeissa. Lisäksi BSCFA:n määrä laski dramaattisesti, kun C2C12 myotuubeja kasvatettiin BCAA-vapaissa olosuhteissa. Näin ollen BSCFA:t olivat todennäköisesti peräisin BCAA-hajotuksesta ja mahdollisesti asyylikoentsyymi A tioesteraasi 9 -entsyymin (ACOT9) toiminnasta. Tulosten pohjalta voidaan todeta, että tulevissa tutkimuksissa olisi tärkeää ottaa elatusaineen ravintoaineiden määrät paremmin huomioon. Jatkotutkimuksissa olisi hyödyllistä selvittää myös asetaatin ja BSCFA:n roolia kudosten välisessä aineenvaihdunnallisessa viestinnässä.

TABLE OF CONTENTS

TERMS AND ABBREVIATIONS

TERMS

Metabolite	An intermediate or end product of metabolism
Metabolite profile	The set of detected and quantified metabolites
Metabolomics	Is the large-scale study of small molecules commonly known as metabolites within a biological sample
Myotube	A multinucleated development stage of mature skeletal muscle fiber. Myotubes are formed by the fusion of myoblasts.

ABBREVIATIONS

ACOT9	Acyl-CoA thioesterase 9
CoA	Coenzyme A
BCAAs	Branched-chain amino acids (isoleucine, leucine & valine)
BSCFAs	Branched short-chain fatty acids (isobutyrate, isovalerate, and 2-methylbutyrate in this case)
DMEM	Dulbecco's modified eagle medium
EPS	Electrical pulse stimulation
HG	High glucose
LDH	Lactate dehydrogenase
LG	Low glucose
TCA cycle	Tricarboxylic acid cycle *i.e.* citric acid cycle

1 INTRODUCTION

Physical activity has been proved to be health-promoting and disease-preventing in many ways (Pedersen and Saltin 2015). However, many of the mechanisms behind the beneficial effects are not well understood. This occurs partly because some of the aspects are difficult and laborious to study in humans or animals. To solve this problem, efforts have been made to develop reliable *in vitro* muscle models that mimic *in vivo* exercise (Carter and Solomon 2019). One of the most promising techniques for modeling muscle contractions and exercise is electrical pulse stimulation (EPS) of the cultured muscle cells (Nikolić *et al.* 2017; Carter and Solomon 2019). Differentiated myotubes like mouse C2C12 myotubes start to contract under influence of EPS (Nikolić *et al.* 2017). EPS has been found to have many similar physiological effects on muscle cells compared with real exercise *in vivo* (Nikolić *et al.* 2017). For example, both approaches increase glucose uptake and oxidation, and secretion of interleukin 6 (Nikolić *et al.* 2012; Evers-van Gogh *et al.* 2015). The EPS approach is particularly useful for finding new potential molecules (e.g. myokines) that affect inter-organ metabolic communication and are secreted from contractile skeletal muscle cells (Raschke et al. 2013).

It is known that active lifestyle and acute exercise affect widely blood and intramuscular metabolite profiles (Kujala *et al.* 2013; Schranner *et al.* 2020; Liu *et al.* 2021). Effects of EPS have been studied previously on certain metabolites like glucose, lactate, and phosphocreatine, but effects of EPS on the wider metabolite profile have been studied only once to our knowledge (Nikolić *et al.* 2017; Hoshino *et al.* 2020). Hoshino *et al.* (2020) studied the effects of acute (60 min) low- and high-frequency EPS on intracellular metabolite profile and transcriptome of C2C12 myotubes. However, there is a large knowledge gap in how chronic EPS affects the intracellular and extracellular metabolite profiles of myotubes. Moreover, the experiments with the C2C12 myotubes are commonly conducted in a culture medium containing supraphysiological 25 mM glucose concentration, while

common blood glucose concentration in mice is between 5.5-11 mM (Fajardo *et al.* 2014). Farmawati *et al.* studied the release of interleukin 6 in response to EPS with C2C12 myotubes in 5 mM and 25 mM glucose media (Farmawati *et al.* 2013). They found that the release was greater under the lower glucose condition suggesting that the effect of glucose level may affect EPS responses.

The primary aim of this work was to find out how chronic (24 h) EPS affects intra- and extracellular metabolite profiles of cultured mouse C2C12 myotubes. Metabolites were analyzed by nuclear magnetic resonance (NMR) spectroscopy. The second aim was to reveal how glucose availability (5.5 mM vs. 25 mM) affects EPS responses.

2 MATERIALS AND METHODS

The differentiated mouse C2C12 myotubes were directed to chronic low-frequency EPS (24 h, 1 Hz, 2 ms, 12 V) to study the effects of *in vitro* model of muscle contraction on myotube and medium metabolite profiles (Figure 1). In addition, the effects of glucose availability were studied by using a low or high glucose culture medium (5.5 mM vs. 25 mM). The metabolites were detected and quantified using NMR spectroscopy-based approach.

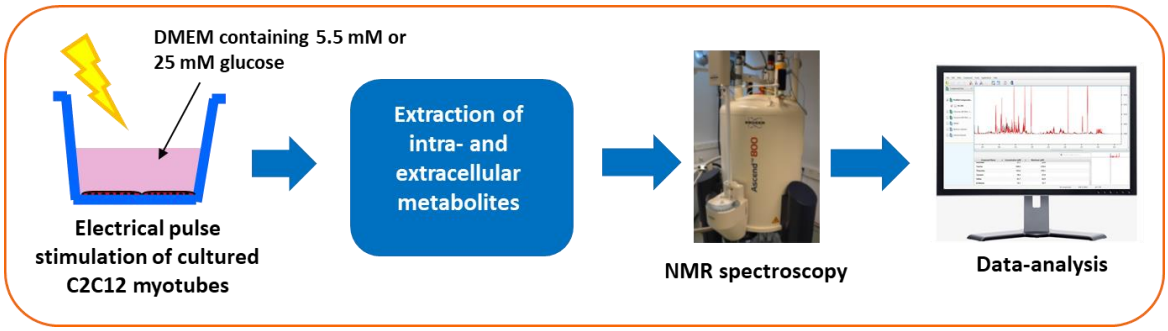

Figure 1. Schematic presentation of the study design.

2.1 Cell culture and differentiation procedure of C2C12 myoblasts

The C2C12 myoblasts (American Type Culture Collection, Manassas, VA, USA) were seeded (≈11 500 cells/cm^2) on regular 6-well plates (Nunclon™ Delta; Thermo Fisher Scientific, Waltham, MA, USA). Passage numbers below eight were used. The growth medium contained high glucose (25 mM) Dulbecco's Modified Eagle Medium (DMEM, #BE12-614F, Lonza, Basel, Switzerland) supplemented with 10% (v/v) fetal bovine serum (FBS, Gibco, Rockville, MD, USA), 2 mM L-glutamine (Lonza), 100 U/ml penicillin and 100 µg/ml streptomycin (Gibco). After 48 hours, the growth medium was switched to high glucose differentiation medium containing 5 % (v/v) FBS, 2 mM L-glutamine, 100 U/ml penicillin, and 100 µg/ml streptomycin. The differentiation medium was replaced every 48 hours.

After four days of differentiation, we switched for half of the cells differentiation medium that contained low glucose (LG, 5.5 mM) DMEM (#12-707F, Lonza), supplemented with 5 % (v/v) FBS, 2 mM L-glutamine, 100 U/ml penicillin, and 100 µg/ml streptomycin. For another half of the cells, we changed fresh high glucose (HG) differentiation medium. According to the manufacturer, the only difference between HG and LG DMEM is the glucose concentration. All the experiments were conducted on day 5-6 post C2C12 differentiation at 37 ˚C and in a 5% CO_2 atmosphere.

2.2 Experimental conditions and electrical pulse stimulation of C2C12 myotubes

After five days of differentiation, the cells were washed twice with phosphate-buffered saline (PBS, Gibco, Thermo Fisher Scientific, USA), and new serum- and antibiotic-free HG or LG DMEM supplemented with 2 mM L-glutamine was added. After a one-hour incubation, the cells were washed once with PBS, and fresh serum- and antibiotic-free HG or LG DMEM containing 2 mM L-glutamine was added. The C2C12 myotubes secrete large amounts of proteins to the medium in response to serum-free conditions (Furuichi *et al.* 2018); moreover, protein secretion by the cells decreases dramatically if the fresh serum-free medium is changed again after one-hour incubation. All the cell experiments were performed in 2 ml of medium.

The EPS was initiated immediately after the second medium change. A commercial electrical pulse stimulator (C-Pace EM 100, IonOptix LLC., Milton, MA, USA) was used in this study. We stimulated the myotubes with low-frequency electrical pulses (1 Hz, 2 ms, and 12 V) for 24 hours. The contractions were visible under an inverted light microscope (Zeiss Axio Vert.A1, Carl Zeiss AG, Germany) approximately after 30 minutes of stimulation.

To yield information on the starting concentrations of the substances in the medium and to ensure that EPS does not have any non-cell mediated effects, fresh high and low glucose medium controls supplemented with 2 mM L-glutamine were incubated for 24 hours with and without EPS (*i.e.* no cells/no power and no cells/power). The sample size was three in these control experiments.

2.3 Extraction of intra- and extracellular metabolites

The intra- and extracellular metabolite extractions were conducted immediately after the EPS (or control time). The metabolic quenching and extraction procedures (Figure 2) were adopted with slight modifications from a tutorial article written by Kostidis *et al.* (2017).

First, the medium from each well was collected and centrifuged for 1 min at 1000xg at +4 °C. Next, 600 µl of pooled medium (three wells were pooled, 200 µl from each) was mixed with 1200 µl of cold methanol (Merck KGaA, Darmstadt, Germany) (Figure 2A). The samples were incubated at -20 °C for 30 minutes after which they were centrifuged for 20 minutes at 16 000xg at +4 °C and the supernatants were stored at -80 °C until drying.

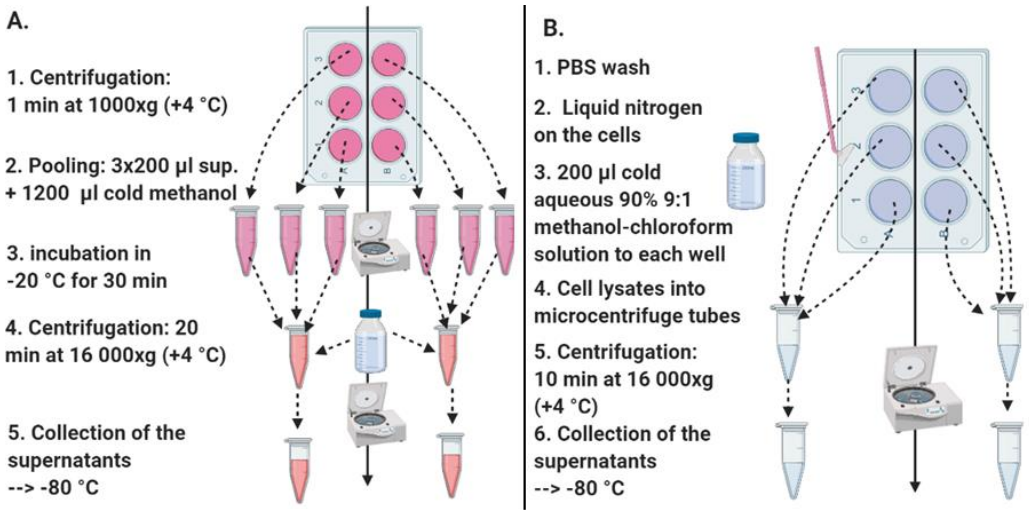

Figure 2. Schematic presentation of the extracellular (A) and intracellular (B) metabolite extraction protocols.

At the same time, the cells were washed once with cold PBS after which liquid nitrogen was added to the wells (Figure 2B). After evaporation of liquid nitrogen, 200 µl of cold 90% (v/v) 9:1 aqueous methanol/chloroform (Sigma-Aldrich, St. Louis, Missouri, USA) solution was added to each well. The cells were scraped with a regular cell scraper and lysates of three wells were pooled to ensure sufficient metabolite concentrations (Figure 2B). The cell lysates were centrifuged for 10 minutes at 16 000xg at +4 °C and supernatants were stored at -80 °C. All the experiments were replicated so that the total sample size was 6-8 per group.

2.4 Sample preparation for NMR spectroscopy

To get rid of methanol and chloroform, samples were dried at room temperature using a vacuum concentrator (Speed Vac Plus SC110A, Savant Instruments Inc., USA) equipped with a vacuum pump (Vacuum pump V-700, Büchi, Switzerland) and controller (Vacuum Controller V-850, Büchi, Switzerland). The drying procedure took 3 hours for the cell extracts and 6 hours for the medium extracts. Dried samples were stored at -80 °C.

To measure the metabolite concentrations, the dried samples were reconstituted with 200 µl of sodium phosphate (Na_2HPO_4-NaH_2PO_4) buffer (150 mM, pH = 7.4) in 99.8% deuterium oxide (D_2O, Acros Organics™, Thermo Fisher Scientific, USA)

containing 0.5 mM 3-(trimethylsilyl)propanesulfonic-d6 acid sodium salt (DSS-d6, IS-2 Internal Standard, Chenomx, Canada). After 30 seconds of vortexing, samples were transferred to regular round bottom 3 mm NMR tubes (Norell Inc., USA).

2.5 NMR experiments, spectral processing, metabolite profiling, and quantification

All the NMR spectra were collected using a Bruker AVANCE III HD NMR spectrometer, operating at 800 MHz ^{1}H frequency (Bruker Corporation, MA, USA) equipped with cryogenically cooled ^{1}H, ^{13}C, ^{15}N triple-resonance probehead. The temperature of the samples was set at 25 °C during the measurements. For the ^{1}H one-dimensional (1D) NOESY experiments, the signal was accumulated with 128 scans per free induction decay (FID), sampled with 133926 complex points covering the spectral width of 16741 Hz, using a relaxation delay of 5 s, acquisition time of 4 s, and mixing time of 0.1 s. The acquisition parameters of the two-dimensional (2D) experiments are provided in Appendix 1.

The Chenomx 8.5-8.6 software (Chenomx Inc., Canada) was used for processing of 1D NMR spectra, metabolite profiling, and quantification. The spectra were automatically zero-filled to the nearest power of two that was at least twice as large as the number of points acquired. Automatic phase correction and baseline (Chenomx Spline) correction were used, and manual adjustments were conducted if necessary. Additionally, Chenomx software's reference peak -based shim correction tool was used to enhance the line shape of the spectra. For each compound was selected a driver peak that was used for quantification (Appendix 2). The internal standard DSS-d6 allowed for fully quantitative analysis.

In addition to ^{1}H 1D spectra, heteronuclear $^{1}H-^{13}C$ heteronuclear single quantum coherence spectroscopy (^{13}C-HSQC) and $^{1}H-^{13}C$ HSQC-total correlation spectroscopy (^{13}C-HSQC-TOCSY), as well as homonuclear $^{1}H-^{1}H$ total correlation spectroscopy (TOCSY) and $^{1}H-^{1}H$ double quantum filtered correlation spectroscopy (DQF-COSY) 2D spectra were used to confirm the identification of the profiled metabolites. The TopSpin 4.0.9 software (Bruker Corporation) was used for

processing (Appendix 1) and analysis of the 2D spectra. Additionally, the identification of isobutyrate, isovalerate, and nicotinate was confirmed by spike-in experiments (Appendix 3). In the spike-in experiments following reagents were used: isobutyric acid (#I1754, Sigma-Aldrich), isovaleric acid (#129542, Sigma-Aldrich), and niacinamide (#47865-U, Sigma-Aldrich).

2.6 Mycoplasma testing

After the experiments, stored medium fractions from the experiments and the used C2C12 cell line (cells from a separate cell culture than in the actual experiments) were tested negative for mycoplasma by a PCR kit (MycoSPY, M020-025, Biontex Laboratories GmbH, München, Germany).

2.7 Lactate dehydrogenase activity, citrate synthase activity, and total protein content measurements

The lactate dehydrogenase (LDH) activity (#981906, Thermo Fisher Scientific) of the medium was measured because its increased activity can indicate cytotoxic effects of EPS (Nikolić *et al.* 2017). The activity of intracellular citrate synthase (#CS0720, Sigma-Aldrich) was measured because differences in its activity can indicate differences in mitochondrial content. The enzyme activities were measured with an automated Indiko plus™ analyzer (Thermo Fisher Scientific). Total protein concentrations (Bicinchoninic Acid Protein Assay Kit, Pierce Biotechnology, Rockford, IL, USA) were measured to ensure that glucose availability or EPS do not affect cell mass which could affect the results. All the assays were conducted according to the manufacturer´s protocol and the enzyme activities in the cells were normalized against total protein content. A discrete cell batch was used for these experiments than in the metabolomics experiments, but the EPS protocol was the same. The total sample size was six in these experiments.

2.8 Small pilot experiment with BCAA-free medium

To see the effects of branched-chain amino acids (BCAAs) on branched short-chain fatty acids, C2C12 myotubes were grown in either standard HG DMEM (Lonza) or

BCAA-free HG DMEM (#1-26S289-I, BioConcept, Allschwill, Switzerland). The sample size was two in these pilot experiments. The medium was collected and analyzed using NMR-spectroscopy as described above.

2.9 Statistical analysis

The 2x2 multivariate analysis of variance (MANOVA) was used to test if there are any main effects or interaction effects between the two explanatory variables**:** EPS and glucose concentration. Tukey's test was used for the pairwise comparisons between LG vs. LG+EPS, and HG vs. HG+EPS. Spearman's rank correlation coefficient was used for measuring statistical dependence. The level of significance was set at $P < 0.05$. IMB SPSS Statistics version 24 was used for the statistical analyses. The results are represented as box-and-whisker plots or mean + standard error of the mean, unless otherwise stated. The heat maps were conducted using the MetaboAnalyst 5.0 platform (https://www.metaboanalyst.ca/).

3 RESULTS

In total 50 distinct compounds were quantified from the C2C12 cells and the medium samples using the NMR spectroscopy-based approach. More specifically, 39 and 37 compounds were quantified from the cells and the medium, respectively. The cell and the medium samples contained 26 common compounds (Figure 3).

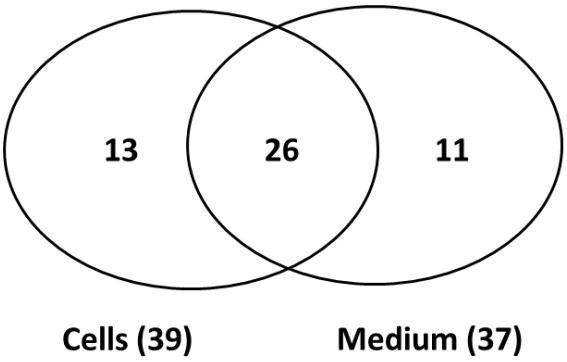

Figure 3. A Venn diagram of the compounds quantified from the cell extracts and the medium samples.

The EPS and glucose availability significantly altered substances in multiple classes such as metabolites related to glycolysis and phosphocreatine system, tricarboxylic acid (TCA) cycle intermediates, branched and straight short-chain fatty acids (BSCFAs and SSCFAs), amino acids, and vitamins. The heat maps demonstrate that in most of the compounds the highest concentrations were observed in the HG+EPS group (Figures 4 & 5).

We also detected 25 compounds from the fresh medium controls and observed that EPS did not affect its composition (Figure 5). Interestingly, the fresh HG medium seems to contain significantly more myo-inositol than the fresh LG medium (Figure 5), even though the manufacturer reports the same concentration for both (Appendix 4). We observed the same trend also in the media that we collected from the actual cell experiments (Figure 5). Another strange observation was that fresh medium contained about 0.75 mM acetate, although according to the manufacturer it does not contain it (Appendix 4).

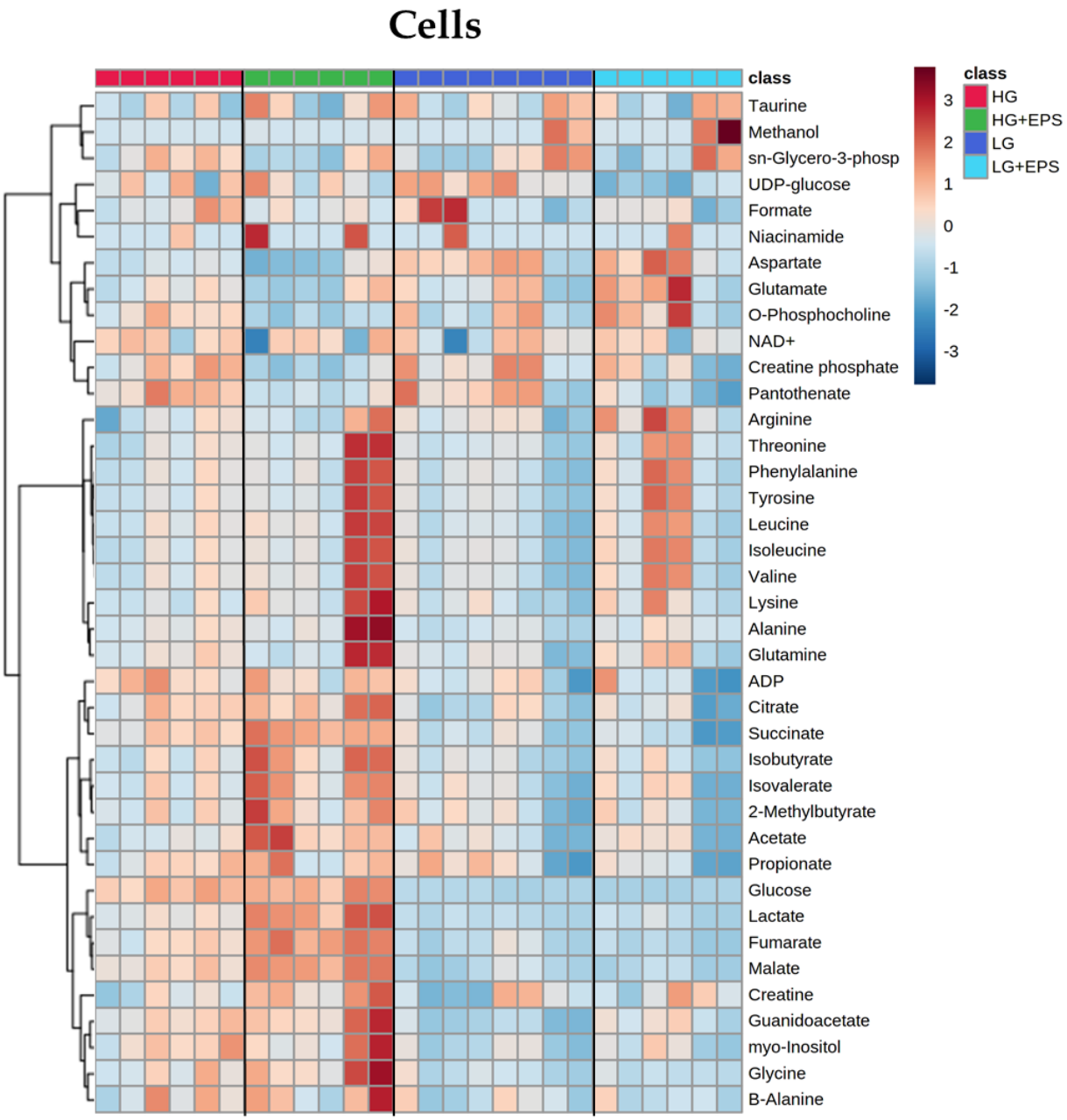

Figure 4. The heat map of the cell extracts. Ward clustering was used for the metabolites (the samples were not reorganized). Darker red/blue equals higher/lower concentration, respectively, relative to other samples. HG/LG = high/low glucose condition, HG/LG + EPS = electrical pulse stimulation (EPS) in high/low glucose condition. Note: it only makes sense to compare the boxes in the same row because autoscaling for the metabolites was used.

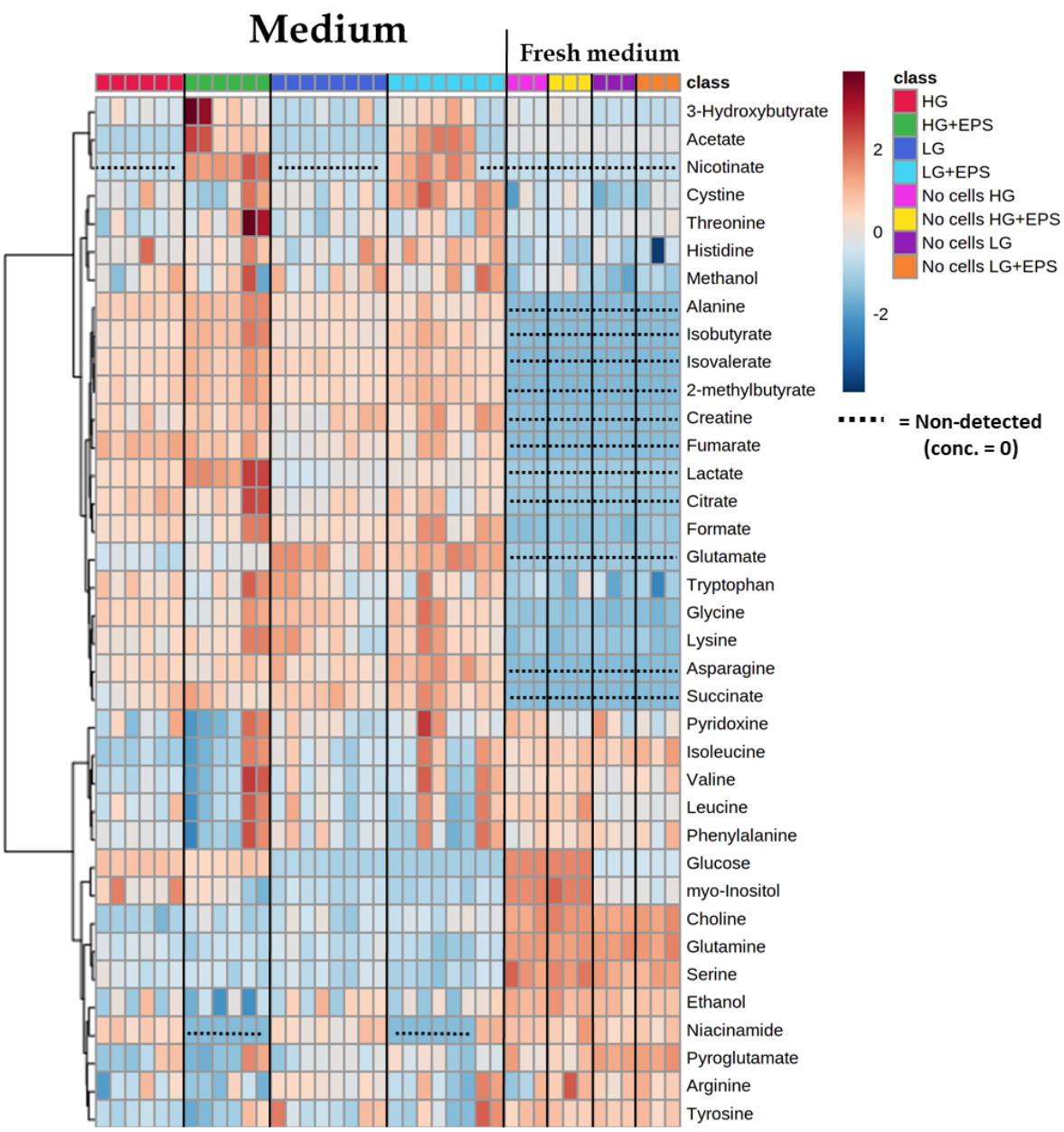

Figure 5. The heat map of the medium samples. Ward clustering was used for the metabolites (the samples were not reorganized). Darker red/blue equals higher/lower concentration, respectively, relative to other samples. HG/LG = high/low glucose condition, HG/LG + EPS = EPS in high/low glucose condition. Note: it only makes sense to compare the boxes in the same row because autoscaling for the metabolites was used.

In the cells, total protein content and citrate synthase activity remained unaltered in response to EPS independent of glucose availability (Figures 6A & 6B). In contrast, both EPS and HG condition increased the LDH activity in the cells (Figure 6C). To evaluate the cell viability, LDH activity was measured also from the medium. In

response to EPS, no differences in the media LDH activity were observed, while higher glucose concentration decreased the LDH activity (Figure 6D).

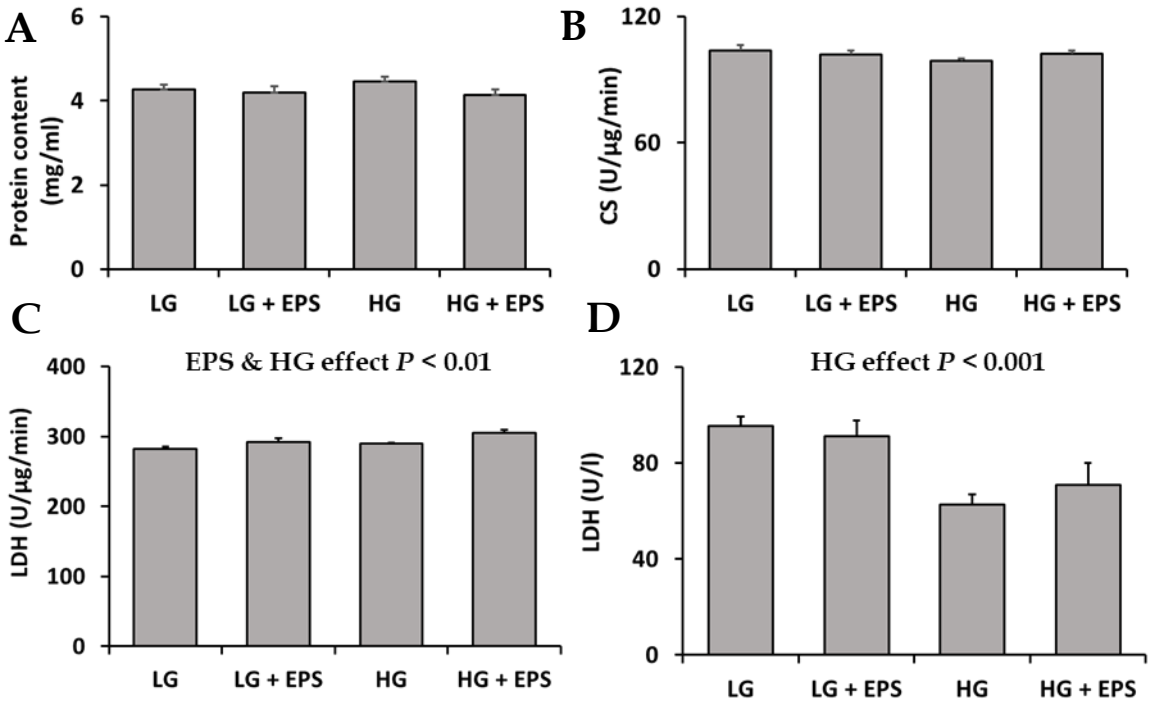

Figure 6. The results of the protein content and enzyme activities. The total protein content (A), citrate synthase (CS) activity (B), and lactate dehydrogenase (LDH) activity (C) in the cells. (D) The LDH activity in the medium samples. Top of each plot is presented results of 2x2 MANOVA if $P < 0.05$. Note: The cells in these experiments (n = 6) were from a different batch from those in the metabolomics experiments.

3.1 EPS influenced metabolites related glycolysis and phosphocreatine system

The chronic low-frequency EPS enhanced glucose consumption in both LG and HG conditions, but the effect was greater in the latter (Figure 7A). In the cells, the production of lactate was increased under HG condition, while lactate content in the medium was increased in both glucose conditions but the increase was greater in HG condition (Figure 7B).

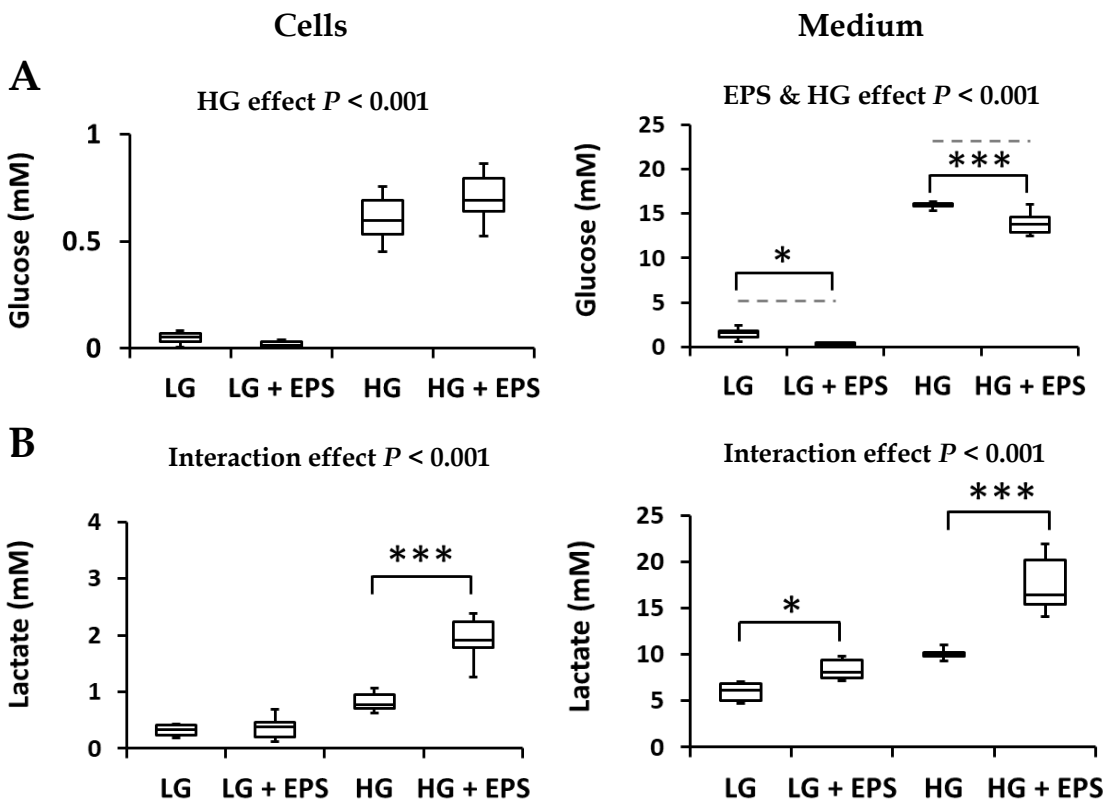

Figure 7. The glucose and lactate concentration of the cell extracts and the medium samples. (A) The glucose concentration in the cell extracts and the medium samples. The dashed lines represent the mean glucose concentrations in the fresh medium control samples. (B) The lactate concentrations in the cell extracts and the medium samples. Top of each graph is presented results of 2x2 MANOVA if $P < 0.05$. Pairwise comparisons between LG and LG+EPS and between HG and HG+EPS were conducted by Tukey's test. * = $P < 0.05$; *** $P < 0.001$. n = 6-8 per group.

The concentration of phosphocreatine decreased significantly in response to EPS in the cell extracts, especially in the HG conditions (Figure 8A). Simultaneously, the dephosphorylated form of creatine increased (Figure 8B), and so the total creatine (phosphocreatine + creatine) remained at the same level (8C). In the medium, the creatine concentration increased in response to EPS but remained low compared to cells (Figure 8D).

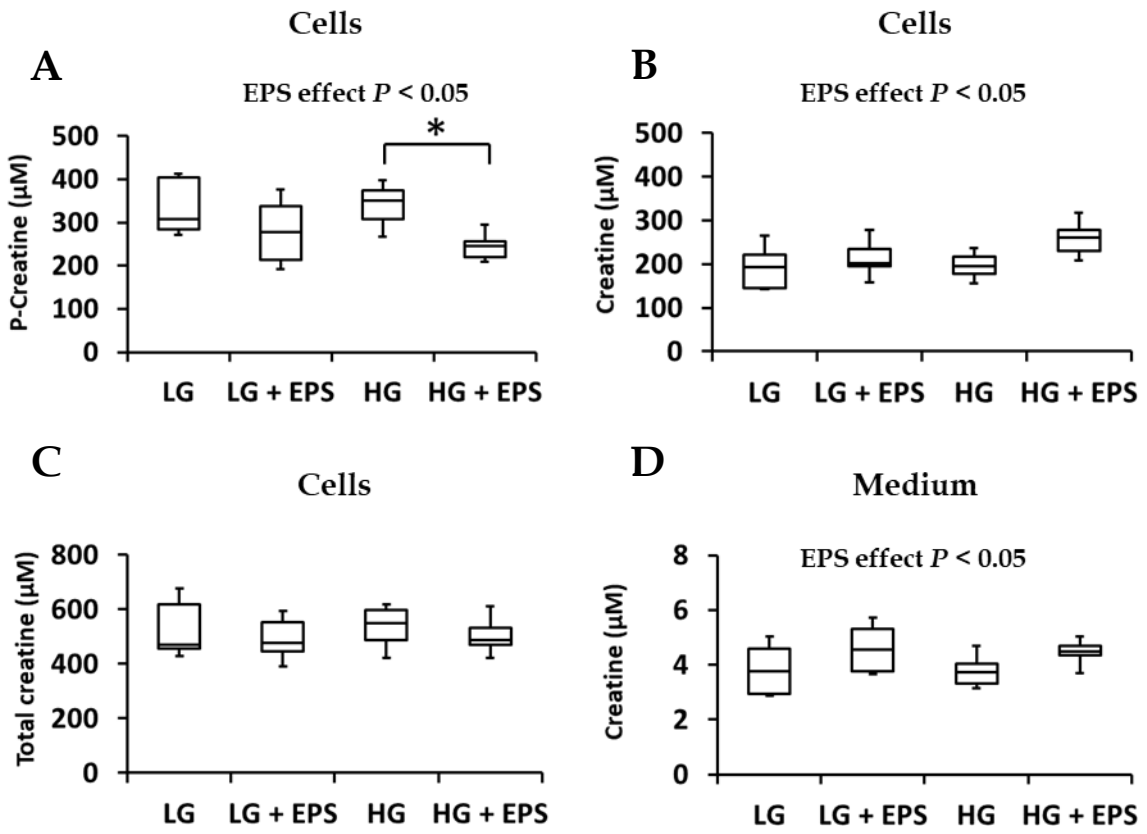

Figure 8. The concentrations of phosphocreatine and creatine. (A) The phosphocreatine concentrations in the cells. (B) The creatine concentrations in the cells. (C) The total creatine concentration (phosphocreatine + creatine) in the cells. (D) The creatine concentration in the medium samples. Top of each plot is presented results of 2x2 MANOVA if $P < 0.05$. Pairwise comparisons between LG and LG+EPS and between HG and HG+EPS were conducted using Tukey's test. * = $P < 0.05$ in Tukey's test. n = 6-8 per group.

3.2 EPS and higher glucose availability alters concentrations of tricarboxylic acid cycle intermediates

In the cells, concentrations of tree TCA cycle intermediates, succinate, malate, and fumarate increased significantly in response to EPS but only in HG condition (Figure 9B-D). In addition, the concentrations of citrate, succinate, fumarate, and malate were higher in HG conditions than in LG conditions (Figure 9A-D). The myotubes released significantly more citrate into the medium in HG than in LG conditions (Figure 9A) and fumarate demonstrated an interaction effect in the medium (Figure 9C).

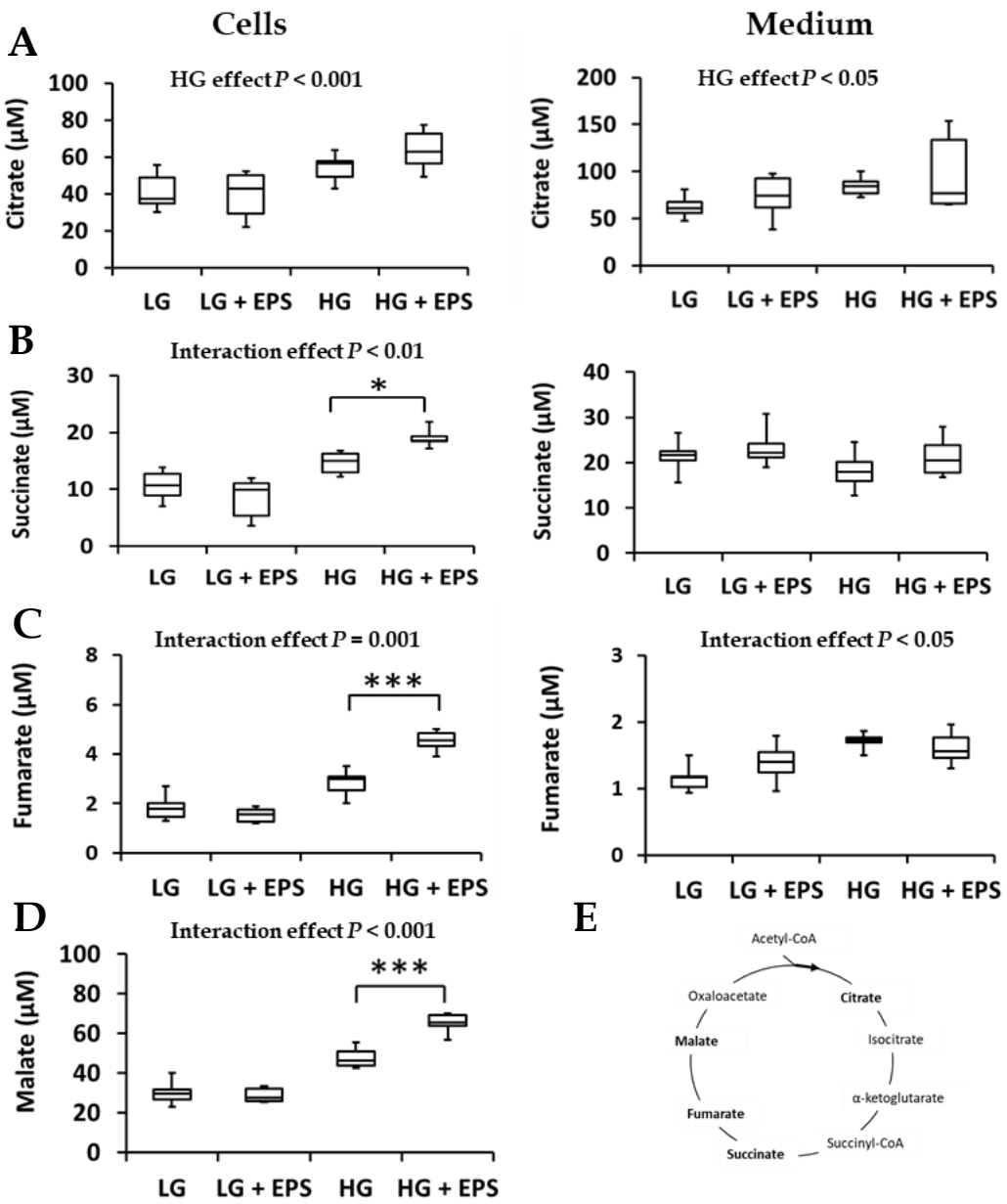

Figure 9. The concentrations of the detected tricarboxylic acid cycle (TCA) intermediates from the cell extracts (left side) and the medium samples (right side). (A) The citrate concentrations in the cells and medium. (B) The succinate concentrations in the cells and medium. (C) The fumarate concentrations in the cells and medium. (D) The malate concentration in the cells. (E) Schematic presentation of the TCA cycle. Top of each plot is presented results of 2x2 MANOVA if $P < 0.05$. Pairwise comparisons between LG and LG+EPS and between HG and HG+EPS were conducted using Tukey's test. * = $P < 0.05$; *** = $P < 0.001$. n = 6-8 per group.

3.3 C2C12 myotubes released acetate into the medium in response to EPS

In response to EPS, intracellular acetate concentration increased in HG condition (Figure 10A), while in the medium acetate concentration increased independent of glucose availability (Figure 10B).

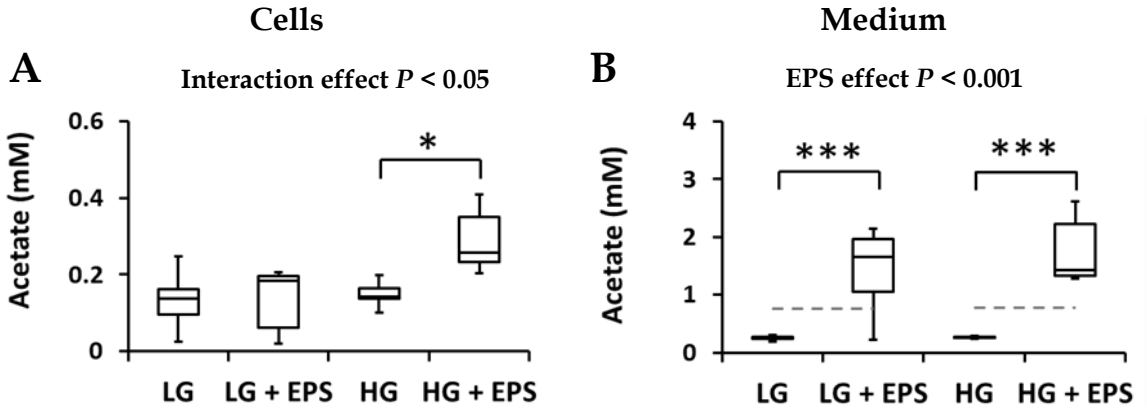

Figure 10. The acetate concentrations in the cell extracts (A) and the medium samples (B). Top of each graph is presented results of 2x2 MANOVA if $P < 0.05$. Pairwise comparisons between LG and LG+EPS and between HG and HG+EPS were conducted using Tukey's test. * = $P < 0.05$; *** = $P < 0.001$. The dashed lines represent the mean concentrations in the cell-free fresh medium control samples. n = 6-8 per group.

3.4 The concentrations of branched short-chain fatty acids and 3-hydroxybutyrate increased in response to EPS and higher glucose availability

We detected three BSCFAs, isobutyrate, isovalerate, 2-methylbutyrate, and one straight SCFA, propionate from the cell extracts (Figure 11A-E). In the cell extracts, isobutyrate and isovalerate concentrations increased significantly in response to EPS and HG condition. In addition, 2-methylbutyrate and propionate concentrations increased significantly in response to the HG condition. The BSFCAs, isobutyrate, isovalerate, and 2-methylbutyrate were also detected from the medium samples. In the medium, the EPS increased significantly concentrations of isobutyrate and 2-methylbutyrate in both LG and HG conditions but especially in HG condition, while the concentrations of isovalerate increased significantly only in HG condition (Figure 11A-C).

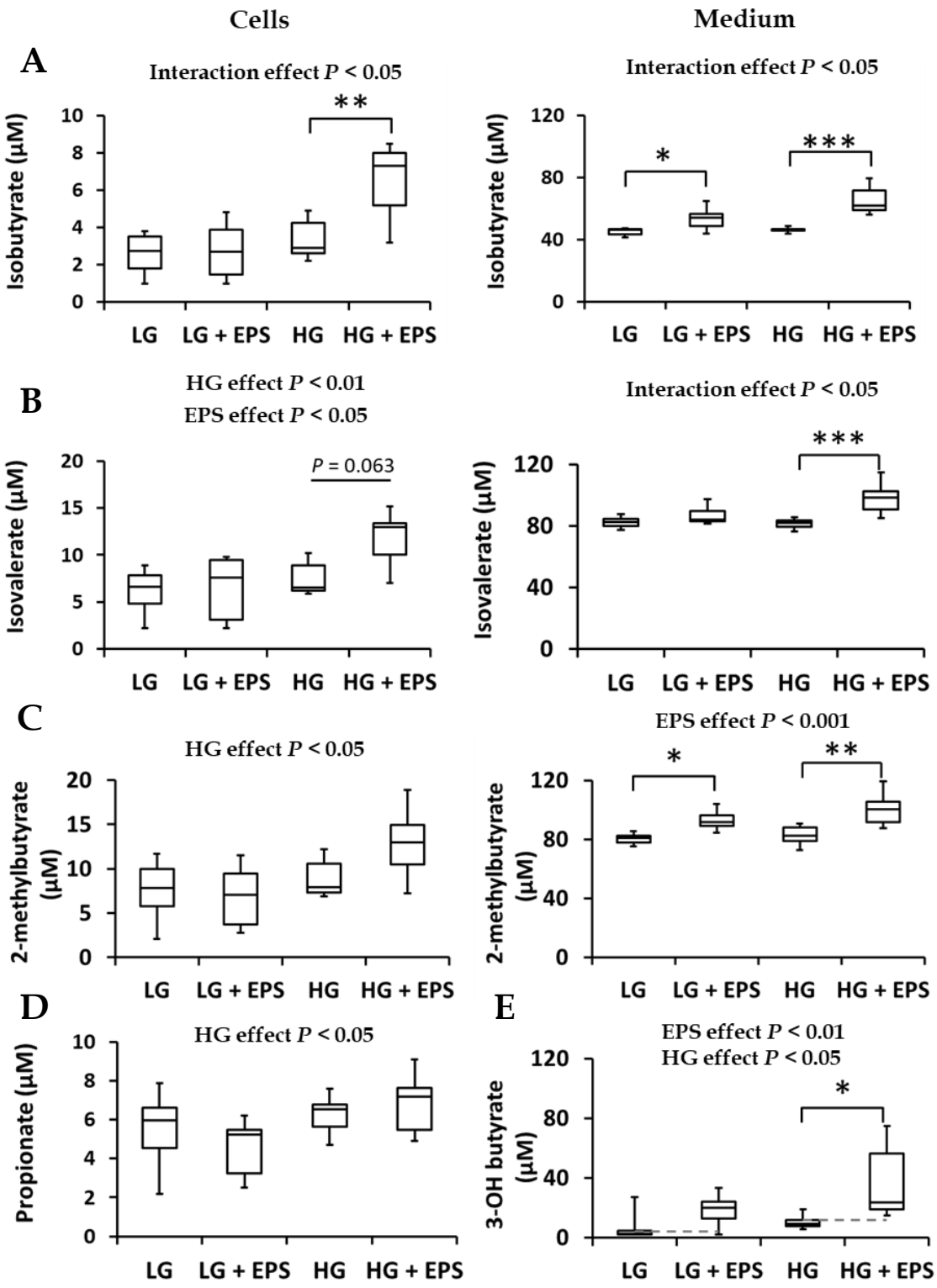

Figure 11. The concentrations of the detected branched and straight short-chain fatty acids and a ketone body 3-hydroxybutyrate from the cell extracts and from the medium samples. (A-C) The isobutyrate, isovalerate, and 2-methylbutyrate concentrations in the cells and the medium. (D) The propionate concentrations in the cells. (E) The 3-hydroxybutyrate concentrations in the medium. Top of each plot is presented results of 2x2 MANOVA if $P < 0.05$. Pairwise comparisons between LG and LG+EPS and between HG and HG+EPS were conducted using Tukey's test. * = $P < 0.05$; ** = $P < 0.01$; *** = $P < 0.001$. n = 6-8 per group.

In addition to BSCFAs, we detected a ketone body 3-hydroxybutyrate from the medium samples. The concentration of 3-hydroxybutyrate increased in response to EPS, especially in HG condition (Figure 11E).

The 3-hydroxybutyrate concentrations in most of the non-EPS samples were about the same level than the background noise from an unknown compound in the fresh medium samples (Figure 11E, Appendix 5). However, the ^{1}H NMR signals of 3-hydroxybutyrate from the EPS samples were very characteristics, and also the ^{1}H—^{1}H TOCSY spectrum supports the identification (Appendix 5).

3.5 Effect of the EPS was greater than the glucose availability on the detected amino acids

We quantified 15 amino acids from the cell extracts and 17 amino acids from the medium samples. In the cells, the concentrations of seven amino acids (isoleucine, leucine, valine, lysine, phenylalanine, threonine, and tyrosine) increased significantly in response to EPS, while glucose availability altered significantly alanine, aspartate, glycine, and β-alanine (Figure 12). Especially aspartate content was greater in LG conditions compared to HG conditions (Figure 13B).

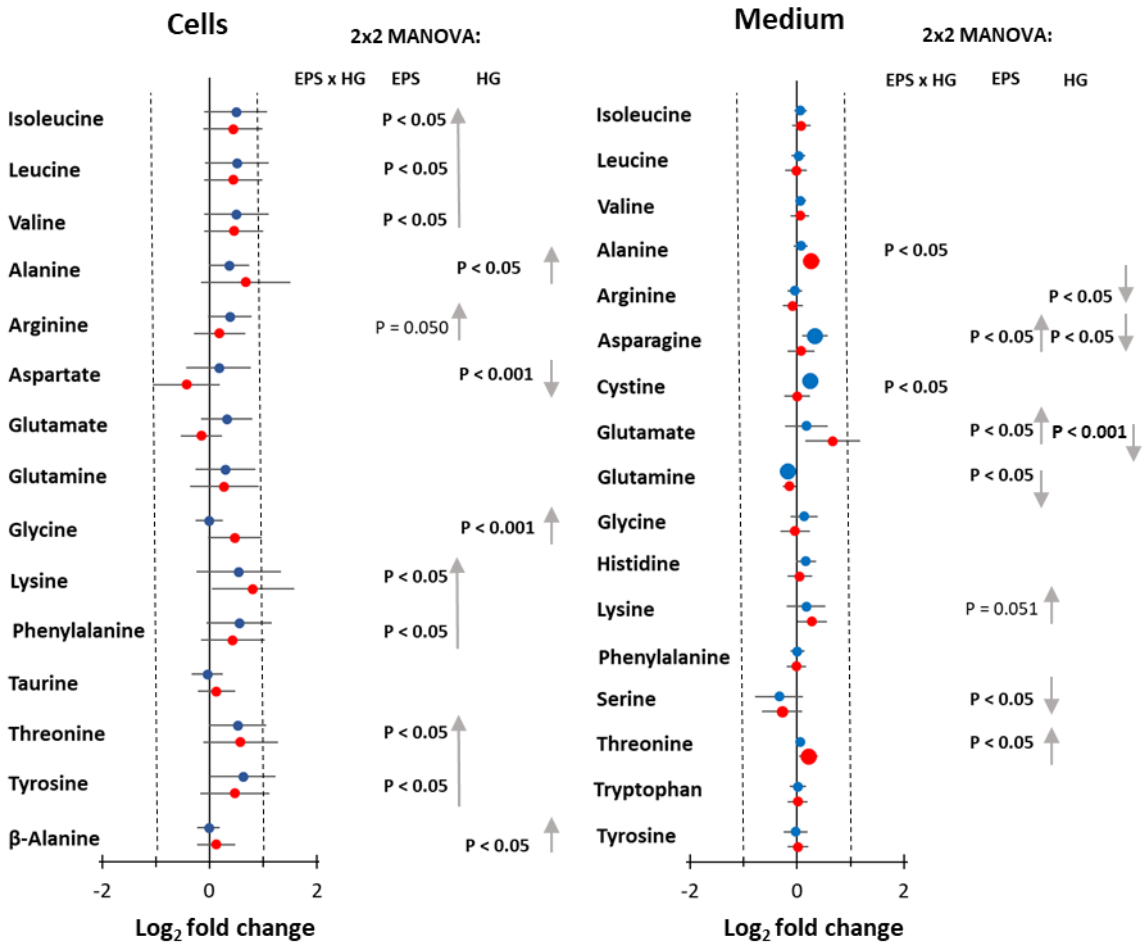

Figure 12. The analyzed amino acids and their fold changes ($\frac{EPS}{no\ EPS}$) with 95% confidence intervals in a $\log_2$ scale. The cell extracts are on the left side and the medium samples on the right side. Blue dot = LG condition. Red dot = HG condition. Next to the plots are represented results of 2x2 MANOVA and the grey arrows show the direction of the main effects. Note: The confidence intervals were calculated using Student's t-distribution while stricter Tukey's test was used for the pairwise comparisons. Bigger dot = $P < 0.05$ in Tukey's test for the EPS-effect in either HG or LG condition. The dashed lines in the plots are to helping in comparison. n = 6-8 per group.

In the media, there were significant increases in asparagine, glutamate, and threonine, and decreases in glutamine and serine in response to EPS (Figure 12). In contrast, concentrations of arginine, asparagine, and glutamate decreased significantly in response to HG condition. The decrease was great especially in glutamate (Figure 13A)

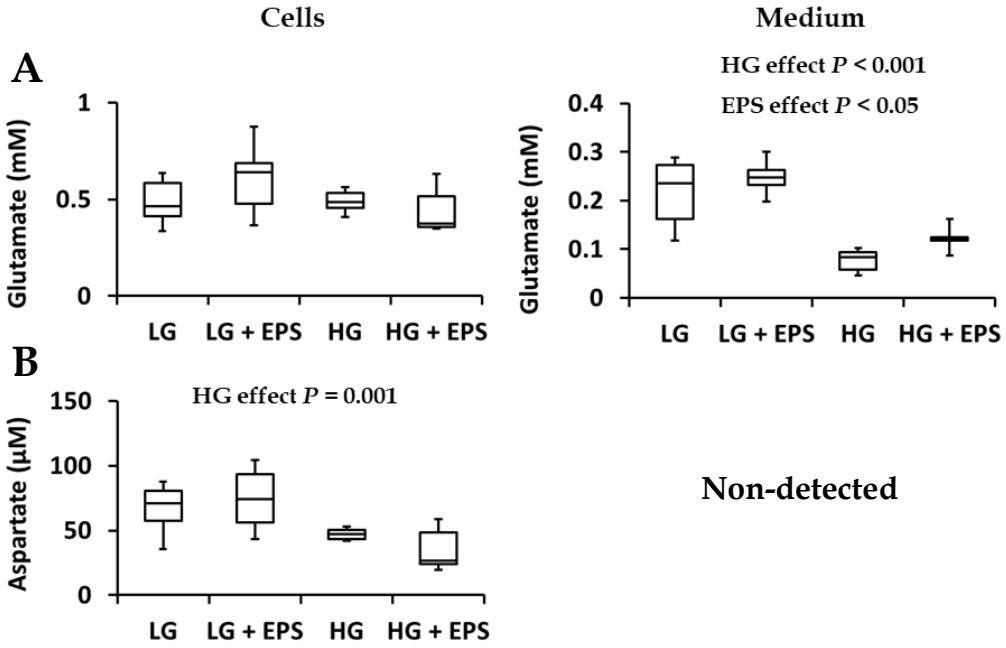

Figure 13. The cells produced more glutamate and aspartate in the low glucose conditions. (A) The glutamate concentrations in the cell extracts and the medium samples. (B) The aspartate concentrations in the cell extracts. Top of each plot is presented results of 2x2 MANOVA if $P < 0.05$. n = 6-8 per group.

The sum of the intracellular BCAAs and the sum of the intracellular BSCFAs showed high correlation (r_s = 0.87), while in the medium they did not correlate (Figure 14A). BSCFAs also highly correlated with each other in the cells and the media (Appendix 6). In the pilot experiment (n=2) where C2C12 myotubes were incubated in a BCAA-free medium, the concentrations of BSCFAs were substantially lower than in normal HG DMEM with BCAAs (Figure 14B).

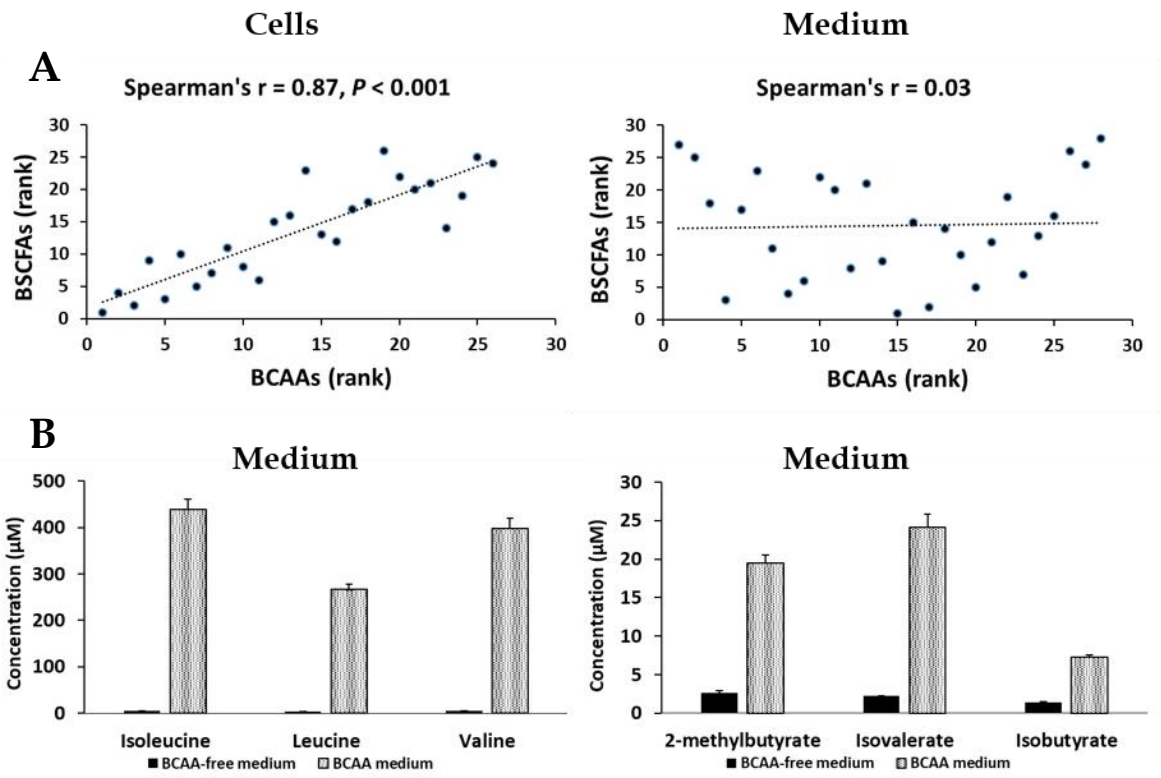

Figure 14. The relationship between branched-chain amino acids (BCAAs) and the branched short-chain fatty acids (BSCFAs). (A) Spearman's rank correlation coefficients between the sum of the BCAAs and the sum of the BSCFAs in the cell extracts (left) and the medium samples (right). (B) The results of the pilot experiment (n = 2) where the C2C12 myotubes were incubated in BCAA-free DMEM or BCAA-containing DMEM. Concentrations of BSCFAs were substantially lower in BCAA-free conditions than in normal DMEM.

3.6 EPS influenced significantly two vitamins: niacin and pantothenate

In the media, niacinamide was converted to nicotinate in 12 of the 14 EPS samples, but not in any of the non-EPS samples (Figure 15). The conversion was verified by a spike-in experiment (Appendix 3). Both compounds are vitamers of B_3.

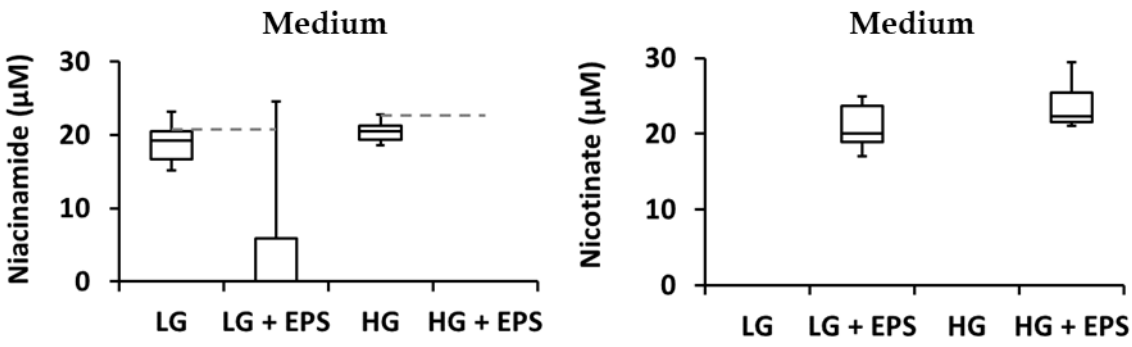

Figure 15. The concentrations of niacinamide and nicotinate, which are two forms of vitamin B_3. In response to EPS, niacinamide was converted to nicotinate in 12 out of 14 samples. The dashed lines represent the mean niacinamide concentrations in the cell-free medium control samples. n = 6-8 per group.

We were also able to quantify two other vitamins: vitamin B_5 (pantothenate) from the cells and vitamin B_6 (pyridoxine) from the media (Figure 16). The concentration of the pantothenate decreased significantly in response to EPS, while pyridoxine remained unaltered (Figure 16).

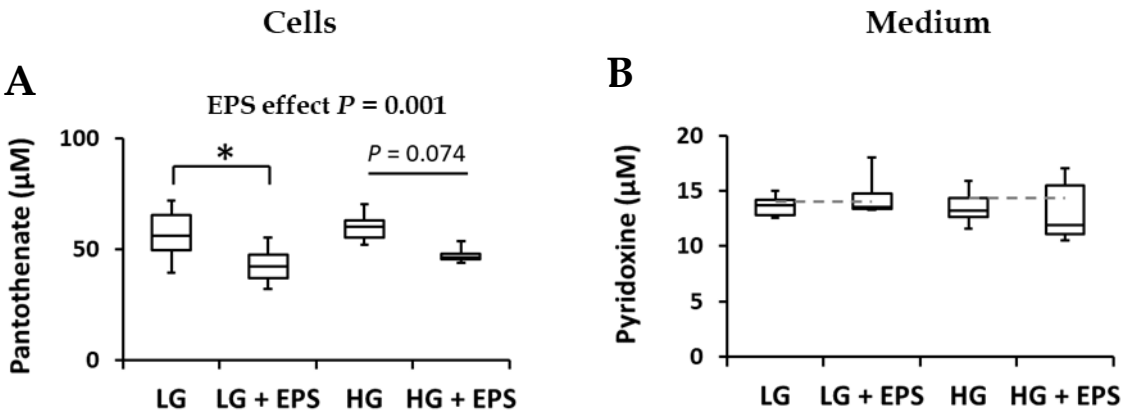

Figure 16. The concentrations of pantothenate and pyridoxine. (A) Pantothenate (vitamin B_5) concentration in the cell extracts. (B) Pyridoxine (vitamin B_6) concentration in the medium samples. The dashed lines represent the mean niacinamide concentrations in the fresh medium control samples. Top of the plot is presented results of 2x2 MANOVA if $P < 0.05$. Pairwise comparisons between LG and LG+EPS and between HG and HG+EPS were conducted using Tukey's test. * = $P < 0.05$. n = 6-8 per group.

4 DISCUSSION

The major aim of the present work was to found out how EPS-induced muscle contractions affect the metabolic responses of C2C12 myotubes. We also wanted to reveal how glucose availability (5.5 mM vs. 25 mM) affects the results. We found that 24-hour low-frequency EPS altered the energy and amino acid metabolism of the mouse C2C12 myotubes, and increased the release of lactate, acetate, BSCFAs, and 3-hydroxybutyrate into the medium. We also found that the EPS did not affect the membrane damage or viability of the cells according to the LDH activity in the

medium (Figure 6D) (Legrand *et al.* 1992). On the other hand, under HG conditions, the cells were possible more viable than under LG conditions according to the LDH activity. However, no other signs of decreased viability were observed. In addition, the EPS or glucose availability did not affect the total protein content of the cells.

4.1 EPS and higher glucose availability increase the metabolic rate of C2C12 myotubes

As expected, the EPS-induced myotube contractions increased the consumption of glucose in both LG and HG conditions. The increased energy production occurred at least partially by increasing anaerobic glycolysis because the lactate production and release were increased. In addition, intracellular lactate dehydrogenase activity increased in response to EPS and HG condition. We also observed that the pantothenate concentration decreased in response to EPS, as others have also observed (Hoshino *et al.* 2020). Pantothenate is needed for coenzyme A (CoA) synthesis (Martinez *et al.* 2014), hence its decrease is also a sign of increased energy consumption.

The C2C12 myotubes secreted large amounts of lactate even at rest and LG condition, meaning that the C2C12 myotubes strongly relies on anaerobic glycolysis for energy production instead of oxidative phosphorylation. After the 24-hour incubation of the cells in LG conditions without EPS, the mean lactate concentration in the medium was 6.0 mM, while the glucose concentration decreased from 5.5 mM to 1.5 mM. It is important to notice that glucose has six carbon atoms and lactate three carbon atoms, and so from one glucose molecule, it is possible to generate (via pyruvate molecules) two lactate molecules (Rabinowitz and Enerbäck 2020). Hence, the cells needed 3 mM glucose to generate that 6 mM lactate. However, there is increasing evidence that lactate is not just a waste product but instead an important fuel and redox buffer at the organismal level (Rabinowitz and Enerbäck 2020). By using the ^{13}C labeled substrates, it has been found that circulating lactate can be a primary source of carbon for the TCA cycle in fed mice (Hui *et al.* 2017).

The phosphocreatine levels in the cells were very similar in the LG and HG conditions at rest. In response to EPS, phosphocreatine concentrations decreased significantly in both LG and HG conditions, but the decrease was greater in HG condition. The phosphocreatine system is the fastest way to resynthesize ATP and it acts as a short-term energy reserve (Guimarães-Ferreira 2014). Hence, compared to the 24-hour low-frequency EPS, phosphocreatine is a more important energy source in very short (<30 s) high-intensity exercise and in stop-and-go sports (Hargreaves and Spriet 2020).

Concentrations of the detected TCA cycle intermediates were higher in HG conditions. Further, concentrations of the detected TCA cycle intermediates increased in response to EPS only in the HG conditions. The concentration of the citrate (1st intermediate) and malate (8th intermediate) were multiple times greater than the concentrations of succinate (6th intermediate) and fumarate (7th intermediate) in every group. In humans, it has been observed that intramuscular resting concentrations of citrate, succinate, and malate are very similar, and their concentrations are multiple times greater than other TCA cycle intermediates (Gibala *et al.* 1998). In humans during exhausting exercise, intramuscular TCA cycle intermediates increase except α-ketoglutarate (Gibala *et al.* 1998).

4.2 C2C12 myotubes release large amounts of acetate in the culture medium in response to EPS

The acetate concentration in the medium increased dramatically during EPS in both LG and HG conditions. It has been observed previously that blood acetate concentration can increase even 9-fold in response to 120 min of knee-extensor exercise (Hall *et al.* 2002). High acetate release is also a marker of overflow metabolism, where cells uptake excessive amounts of substrates but only partially catabolize them (Liu *et al.* 2018; Bose *et al.* 2019).

From pyruvate, acetate can be produced by two mechanisms: (1) enzymatically by ketoacid dehydrogenases and (2) non-enzymatically by reactive oxygen species (ROS) mediated pyruvate decarboxylation (Liu *et al.* 2018) (see Figure 17). Also,

certain acyl-CoA thioesterases hydrolyze acetyl-CoA to acetate and CoA in the liver but possibly also in other tissues as well (Horibata *et al.* 2013; Tillander *et al.* 2014). One another way to release acetate is the deacetylation of acetylated proteins such as histones (Bose *et al.* 2019).

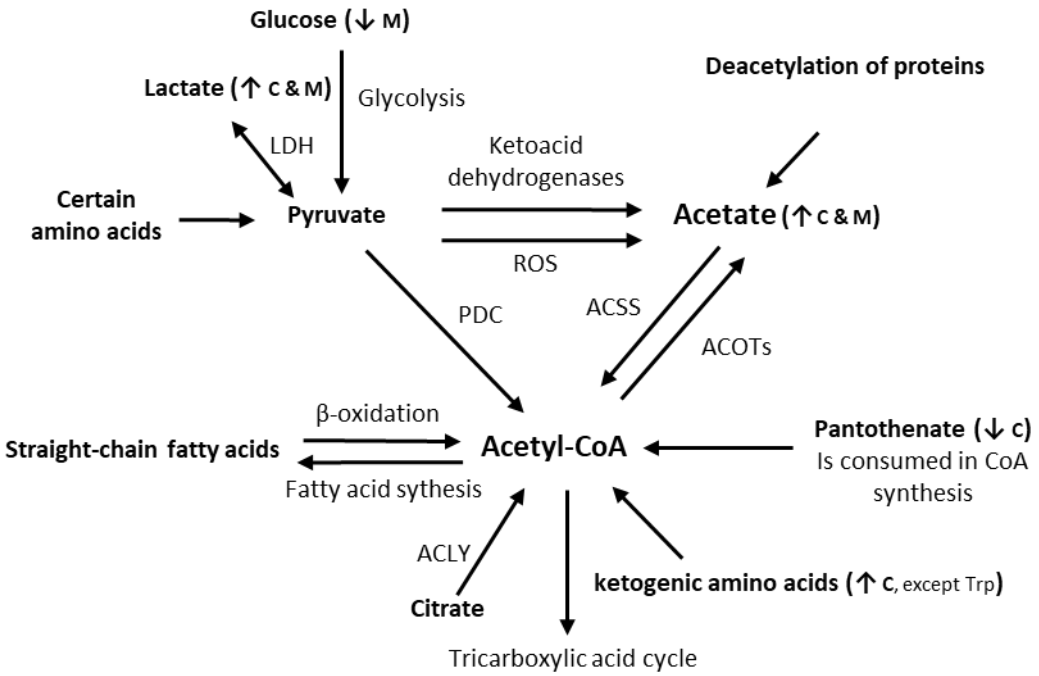

Figure 17. The major pathways to generate acetate and acetyl-CoA in the cells. The arrows in parentheses indicate if the concentration changed in the cells (C) and/or medium (M) significantly in 2x2 MANOVA in response to EPS. ACLY = ATP citrate lyase, ACOTs = acyl-CoA thioesterases, ACSS = acetyl-CoA synthetase, LDH = lactate dehydrogenase, PDC = pyruvate dehydrogenase complex, ROS = reactive oxygen species. The figure is adapted from (Bose *et al.* 2019).

ROS contributes around 5-15% of the acetate under typical cell culture conditions (Liu *et al.* 2018). However, it has been shown that EPS (>45 min) of the C2C12 myotubes causes the accumulation of ROS (Pan *et al.* 2012; Horie *et al.* 2015). Therefore, the accumulation of ROS may be an important or even the major reason behind the high media acetate concentrations in response to EPS. ROS are also generated by contractile skeletal muscles in humans and other animals, and intense and prolonged exercise can cause oxidative damage to different cellular components (Powers *et al.* 2020). However, ROS accumulation is needed for many

exercise-mediated adaptations, such as mitochondrial biogenesis (Powers *et al.* 2020).

In the future, it would be interesting to introduce ROS such as hydrogen peroxide into the medium, and measure acetate concentrations in cells and media. Also, it would be a good idea to measure ROS content and activity of the ketoacid dehydrogenases after the EPS protocol. In addition, acetate's role in inter-organ metabolic communication would be beneficial to study more.

Independent of the EPS, we also observed that fresh (cell-free) medium samples contained 0.74 to 0.79 mM acetate. Others have also reported similar findings, and there is evidence that pyruvate can convert non-enzymatically to acetate in DMEM (Kamphorst *et al.* 2014; Vysochan *et al.* 2017). We did not detect pyruvate from the medium although it should contain 1.0 mM it (Appendix 4). Hence, probably the non-enzymatic conversion of pyruvate to acetate is occurring in this case.

4.3 C2C12 myotubes release BSCFAs and 3-hydroxybutyrate, catabolic products of branched-chain amino acids, into the medium

The secretion of three BSCFAs, isobutyrate, isovalerate, and 2-methylbutyrate increased in response to EPS (Figure 11A-C). In blood, their origin is usually considered to be from intestinal microbes (Jakobsdottir *et al.* 2013). However, rodents and humans express the mitochondrial acyl-CoA thioesterase 9 (ACOT9) enzyme that seems to be capable to convert certain catabolic products of amino acids to BSCFAs, straight short-chain fatty acids (SSCFAs), and acetate (Tillander *et al.* 2014). From the BCAAs (valine, leucine, and isoleucine) compounds named isobutyryl-CoA, isovaleryl-CoA, and 2-methylbutyryl-CoA can be produced, respectively (see Figure 18)(Crown *et al.* 2015; Wallace *et al.* 2018). If the ACOT9 thioesterase hydrolyses these compounds, it generates isobutyrate, isovalerate, 2-methybutyrate, and CoA. Tillander *et al.* (2014) found that mouse ACOT9 had the following V_{max} values for isobutyryl-CoA and isovaleryl-CoA: 31.9 ± 7.9 µmol/min/mg and 15.0 ± 0.1 µmol/min/mg, respectively. The observed high correlation between intracellular BCAAs and BSCFAs and the results of the pilot

experiment with BCAA-free medium supports the interpretation that the detected BSCFAs were derived from the BCAAs (Figure 14).

Tillander *et al.* (2014) found that the ACOT9 enzyme was produced only in low amounts in mouse skeletal muscle tissue (Tillander *et al.* 2014). On the other hand, others have observed that the ACOT9 enzyme is highly produced in mouse skeletal muscle tissue (Bekeova *et al.* 2019). It has been suggested that ACOT9 provides a regulatory link between mitochondrial fatty acid and amino acid metabolism (Tillander *et al.* 2014), and the observed high correlation between intracellular BCAAs and BSCFAs supports the suggestion.

In adipocytes, BSCFAs are used for synthesizing longer monomethyl branched-chain fatty acids (mmBCFAs) (Wallace *et al.* 2018). It has been found that mmBCFA content in adipose tissue correlates positively with skeletal muscle insulin sensitivity (r_s=0.59), and after weight loss, mmBCFA content in adipose tissue increases significantly (Su *et al.* 2015). Therefore, the present findings suggest that skeletal muscles may feed BSCFAs to adipocytes where they can be used for monomethyl branched-chain fatty acid synthesis, but this is needed to confirm *in vivo* in the future.

It has been earlier observed that C2C12 cells express the *ACOT9* gene (Zhou *et al.* 2012) but it would be important to also measure the enzyme activity of the ACOT9 in C2C12 myotubes after the EPS in the future. It would be also interesting to reveal the role of BSCFAs in inter-tissue metabolic communication *in vivo*.

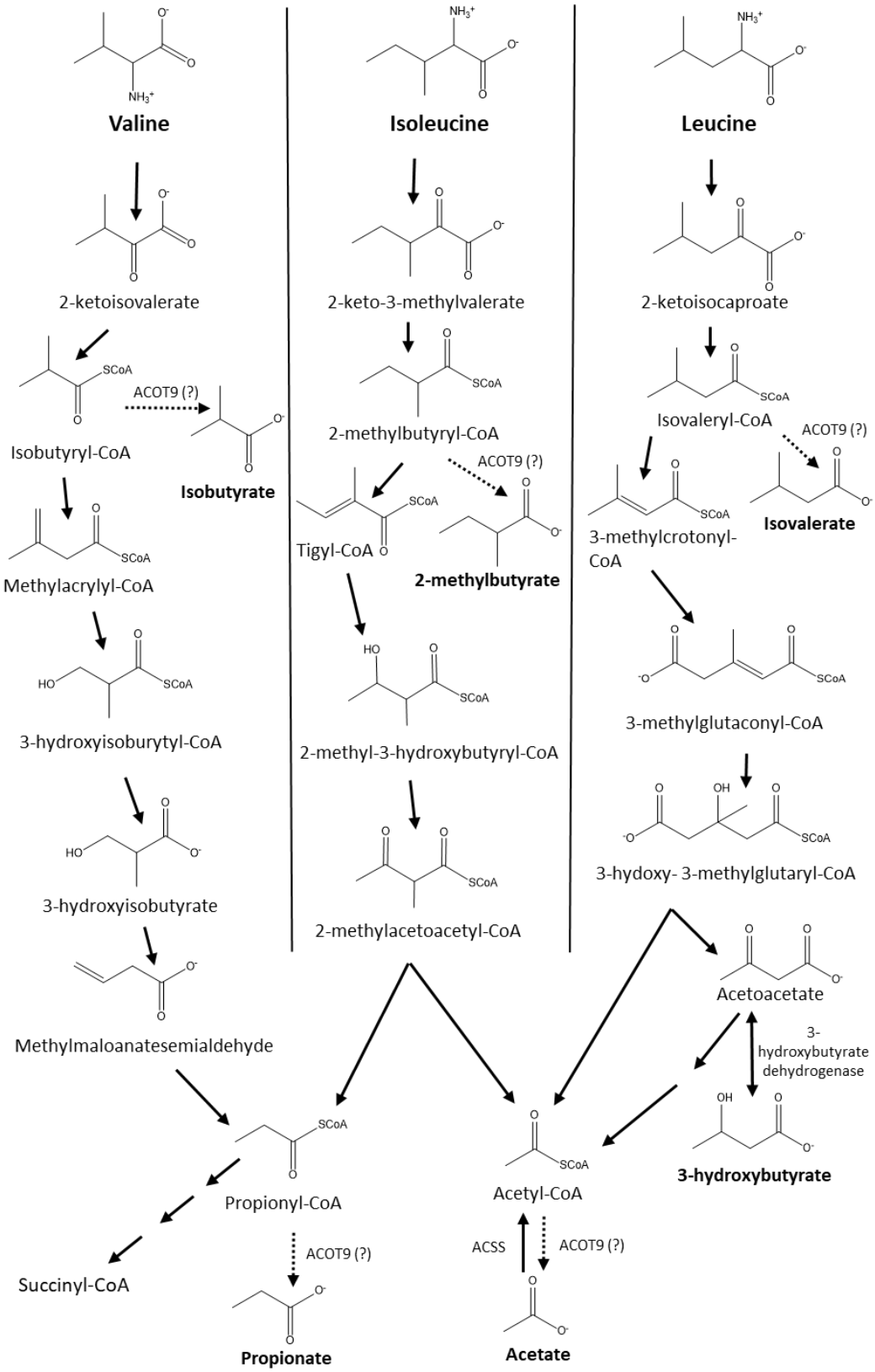

Figure 18. Catabolic pathways of branched-chain amino acids (BCAAs). The bolded compounds were detected from the cell extracts and/or the medium samples. ACOT9 = acyl-CoA thioesterase 9, ACSS = acetyl-CoA synthetase. The dashed arrow reflects the hypothesis that the isobutyrate, 2-methylbutyrate, isovalerate, and propionate were formed in the C2C12 myotubes from the action of the ACOT9 enzyme. The figure is adapted from Crown *et al.* (2015).

We also observed that the concentration of the ketone body 3-hydroxybutyrate increased in the medium in response to EPS. During and after exercise, the concentration of the 3-hydroxybutyrate has been shown to increase in blood in numerous studies with humans (Schranner *et al.* 2020). It has been suggested that the increased 3-hydroxybutyrate concentration in blood may reflect a metabolic shift from usage of carbohydrates towards fats and ketones (Morville *et al.* 2020). 3-hydroxybutyrate is generated from acetoacetate, and the reversible reaction is catalyzed by the 3-hydroxybutyrate dehydrogenase (*BDH1,* Figure 19) (Newman and Verdin 2017). Acetoacetate can break down spontaneously into acetone that evaporates easily (Hay and Bond 1967), hence acetoacetate and acetone were possible lost in the drying procedure. In addition to ketogenesis in the liver, acetoacetate is formed in muscles from the catabolism of leucine (see Figure 18) (Shimomura *et al.* 2004). Acetoacetate is formed also from the catabolism of phenylalanine and tyrosine, but this occurs mainly in the liver (Lerner 1949).

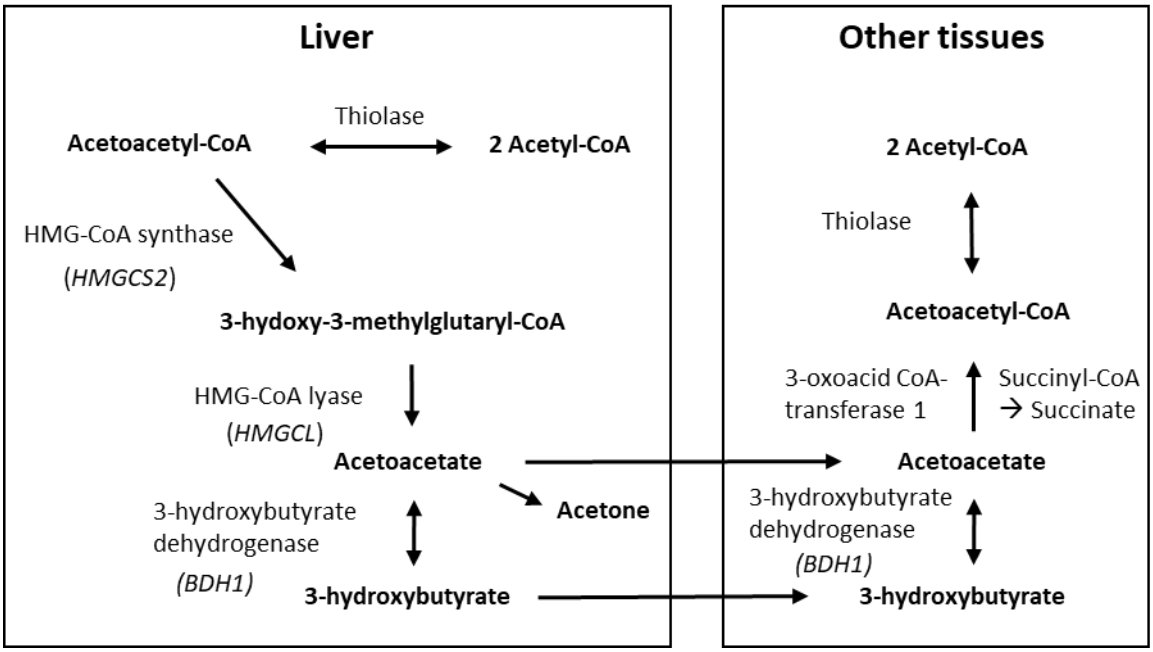

Figure 19. A schematic presentation of the ketogenesis in the liver and usage of ketone bodies in other tissues. In parentheses are presented gene names of certain enzymes. The figure is adapted from Nelson and Cox (2013).

The 3-hydroxybutyrate concentration has been increased also in the interstitial fluid of skeletal muscle in both humans and rats after endurance exercise (Zhang *et al.* 2019). Albeit, *in vivo* situations, it is generally regarded that the 3-hydroxybutyrate is released from the liver (Newman and Verdin 2017). However, small amounts of 3-hydroxybutyrate may be released also from working skeletal muscles (at least *in vitro* situations). Gene expression of 3-hydroxybutyrate dehydrogenase (*BDH1*, see Figure 19) in skeletal muscles has been greater in trained mice compared to sedentary mice (Svensson *et al.* 2016). Also, in some studies with humans, *BDH1* expression is increased in response to acute exercise, while meta-analysis of skeletal muscle response to exercise (MetaMEx) search indicates that inactivity decreases *BDH1* expression (MetaMEx 2020; Pillon *et al.* 2020). It is also found that muscle-specific overexpression of proliferator-activated receptor γ coactivator 1α (*PGC-1a*) increases gene expression of *BDH1* in mice (Svensson *et al.* 2016). PGC-1α is an important regulator in exercise-induced mitochondrial biogenesis (Lira *et al.* 2010). In C2C12 myotubes, the transcription and translation of *PGC-1a* have been increased after 24-hour EPS (Burch *et al.* 2010). Therefore, these findings may indicate that EPS can increase the expression and activity of BDH1, and this way increase the formation of 3-hydroxybutyrate from acetoacetate. Therefore, the next step in the future would be to determine the enzyme activity of the BDH1 after the EPS.

Also, it is possible that the ketogenic pathway can be slightly active also in other tissues than in the liver. An important regulatory enzyme in the 3-hydroxybutyrate synthesis pathway, 3-hydroxy-3-methylglutaryl-CoA synthase 2 (*HMGCS2,* see Figure 18) is highly expressed in the liver but the *HMGCS2* gene is also expressed in other tissues, such as in skeletal muscles in humans (Newman and Verdin 2017). According to the MetaMEx search, the *HMGC2* gene expression increases significantly in skeletal muscles in humans after acute high-intensity training and acute resistance training (MetaMEx 2020; Pillon *et al.* 2020). Also, another gene, *HMGCL* that is needed for ketogenesis (see Figure 18), is expressed in at least small amounts in skeletal muscles in humans (MetaMEx 2020; Pillon *et al.* 2020). Therefore, it would be interesting to measure enzyme activities of HMGCS2 and

HMGCL after the EPS. Indeed, the RNASeq analysis of myotubes is currently investigated.

4.4 EPS and glucose availability alters the amino acid composition of the C2C12 myotubes and the media

In human studies when blood has been collected 0-0.5 hours after exercise, alanine, leucine, and isoleucine have shown a consistent response, while the results have been contradictory for the other proteinogenic amino acids (Schranner *et al.* 2020). Blood alanine concentration typically increases in response to an acute bout of resistance and endurance exercise (Schranner *et al.* 2020). On the other hand, blood leucine and isoleucine concentrations typically decrease after acute exercise (Schranner *et al.* 2020). The C2C12 myotubes secreted significantly more alanine into the medium during EPS under HG condition, while there were no differences between groups in the mediua concentrations of leucine or isoleucine. However, there were significant increases in the intracellular concentrations of leucine and isoleucine (and third BCAA, valine) in response to EPS, suggesting that protein degradation was increased. Similar findings have been observed in type II glycolytic (but not in type I oxidative) muscle fibers immediately after acute resistance exercise (Blomstrand and Essén-Gustavsson 2009).

Glucogenic amino acids can be degraded to pyruvate and then transaminated to alanine. Blood delivers alanine into the liver where it is converted back to pyruvate and further to glucose (Schranner *et al.* 2020). Then the glucose is delivered to other tissues by circulation, *i.e.* alanine-glucose cycle. Leucine, isoleucine, and third BCAA, valine, are degraded during exercise to isovaleryl-CoA, 2-methylbutyryl-CoA, and isobutyryl-CoA, respectively (Shimomura *et al.* 2004). These compounds can be further processed to succinyl-CoA and/or acetyl-CoA (Shimomura *et al.* 2004), or hydrolyze to isovalerate, 2-methylbutyrate and isobutyrate as now observed.

There was prominently more glutamate in the media in LG than in HG condition. In mammals, glutamate is typically generated from glutamine by glutaminase

enzyme (Newsholme *et al*. 2003). Interestingly, we did not observe differences in the glutamine concentrations in response to glucose availability. However, glutamate can be generated also from a TCA cycle intermediate, α-ketoglutarate at least by two different mechanisms: (1) α-ketoglutarate + NH_3 ⇌ Glutamate + H_2O by glutamate dehydrogenase, and (2) α-ketoglutarate + alanine ⇌ Glutamate + pyruvate by alanine transaminase (Newsholme *et al.* 2003). In addition, intracellular aspartate content was significantly higher in LG than in HG conditions. Aspartate is also an amino acid that can be synthesized from a TCA cycle intermediate, oxaloacetate (Nelson and Cox 2013). Aspartate aminotransferase catalyzes the following reaction: oxaloacetate + glutamate ⇌ aspartate + α-ketoglutarate (Nelson and Cox 2013). The differences in glutamate and aspartate content between the LG and HG condition can be due to two reasons: (1) glutamate and aspartate are generated more in LG condition or (2) they are consumed more in HG condition. One would need to use some other method like ^{13}C-fluxomics for answering that question. However, the present results suggest that glutamate and aspartate seem to have important roles in the metabolism of C2C12 myotubes when glucose availability is modulated.

4.5 Strengths and limitations of the study

The present study contains four major strengths. (1) To our knowledge, this study was the first one where was studied how EPS affects both intra- and extracellular metabolite profiles. The approach provides important information on which metabolites are primarily secreted and which are primarily taken up to cells. (2) Effects of glucose availability on EPS results have been studied in a very limed number of studies, although glucose availability is known to modulate many intramuscular processes (MacDonald *et al.* 2020). (3) ^{1}H NMR spectroscopy enabled fully quantitative analysis, which helps to understand the scale of changes between different metabolites. (4) Finally, the fact that we used an almost identical EPS program that has been used in multiple studies (*e.g.* Raschke *et al.* 2013; Görgens *et al.* 2013, 2016; Evers-van Gogh *et al.* 2015), helps to place the results in a broader context.

There are three important limitations in the present study. (1) Unstimulated cells were incubated without carbon electrodes, although EPS has been reported having non-cell mediated effects on the medium also which has affected on certain cellular processes (Evers-van Gogh *et al.* 2015). However, we aimed to compensate for this limitation by including stimulated and unstimulated fresh media controls in the study and we did not observe non-cell mediated changes in their composition. (2) Because of the drying procedure (to get rid of methanol/chloroform), some unstable or volatile metabolites such as acetoacetate and acetone were possibly lost. (3) Low-concentrated metabolites (< 1 μM) were not detected, so in the future, it would be beneficial to perform mass spectrometry analysis alongside NMR spectroscopy. In addition, dynamic metabolomics *i.e.,* fluxomics would help in answering many questions.

4.6 Concluding remarks

We found that EPS-induced myotube contractions enhanced the glucose utilization and release of lactate, acetate, BSCFAs, and 3-hydroxybutyrate from the C2C12 myotubes (Figure 20). Many of the metabolic responses were stronger or occurred only when glucose availability was higher. Hence, it would be wise to consider the nutritional load in future EPS experiments. In addition, the metabolism of the C2C12 myotubes resembles type II glycolytic muscle fibers according to the increased lactate release and the increased intracellular BCAA content in response to EPS. Lastly, the secretion of acetate and BSCFAs would be important to be confirmed using *in vivo* settings because they may have important roles in inter-organ metabolic communication.

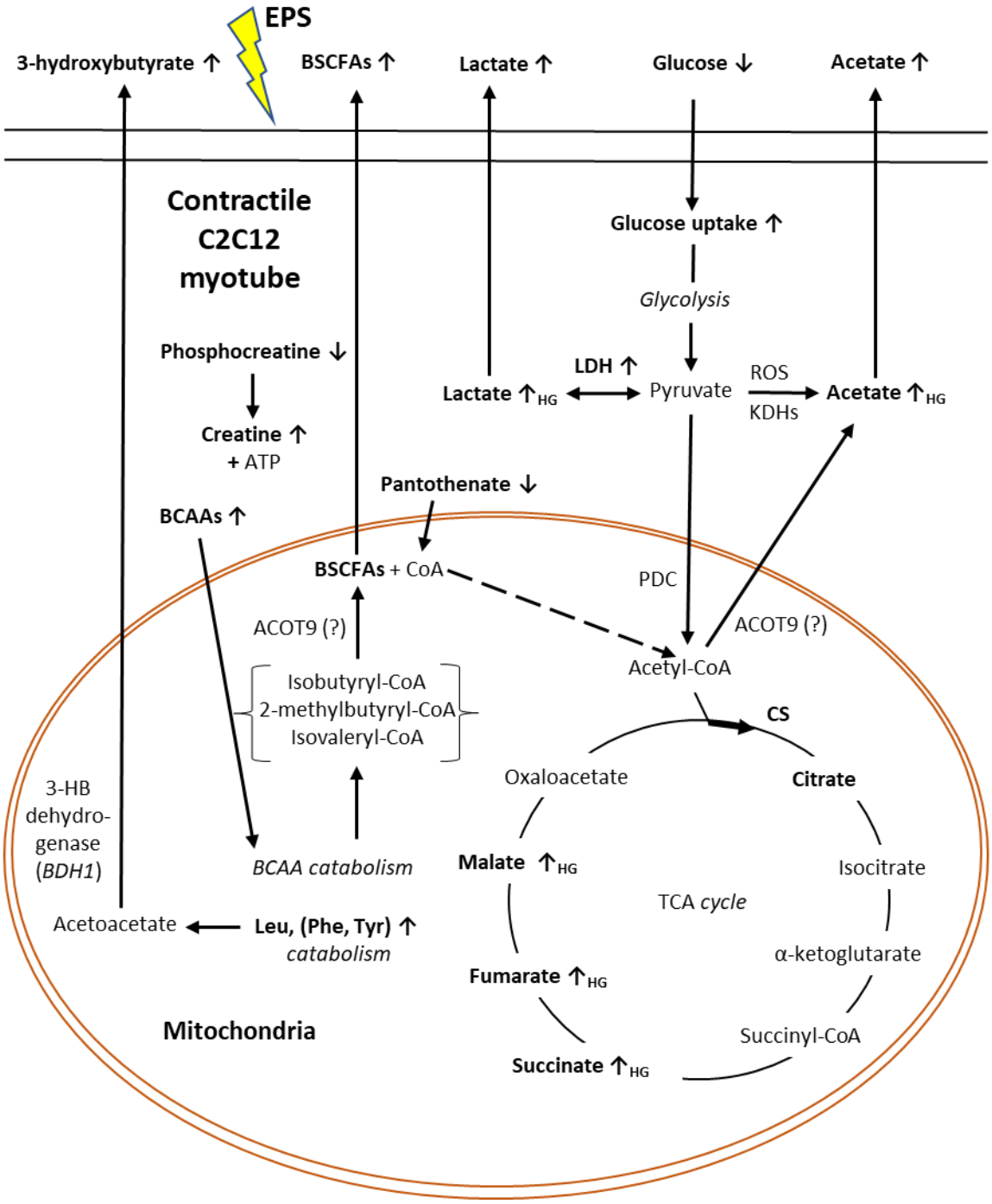

Figure 20. Schematic summarization and interpretation of the main EPS effects on the metabolism of the C2C12 myotubes. EPS increased glucose utilization via the glycolytic pathway. Generated pyruvate was converted into lactate by the lactate dehydrogenase (LDH) enzyme and into acetate possible by reactive oxygen species (ROS) and ketoacid dehydrogenases (KDHs). The C2C12 myotubes secreted branched short-chain fatty acids (BSCFAs, isobutyrate, 2-methylbutyrate & isovalerate) in the medium. BSCFAs were possible generated through hydrolysing intermediates from the catabolic pathway of branched-chain amino acids (BCAAs) by acyl-CoA thioesterase 9 (ACOT9). The C2C12 myotubes also released a ketone body 3-hydroxybutyrate into the medium, which was possibly formed through catabolism of leucine. Only the bolded metabolites and enzymes were detected or analyzed. The arrow after the metabolite or enzyme indicates whether it

increased or decreased in response to EPS. $\uparrow_{HG}$ = EPS effect was observed only in high glucose condition. CS = citrate synthase, PDC = pyruvate dehydrogenase complex.

ACKNOWLEDGEMENTS

I want to thank my supervisors, Associate Professor Juha Hulmi and Professor Perttu Permi, who made this project possible. Juha Hulmi launched the project and Perttu Permi operated the NMR Spectrometer and instructed me in the interpretation of 2D spectra. I also want to give special thanks to my mentors, Associate Professor Thomas O'Connell, and doctoral researcher Juulia Lautaoja. Thomas O'Connell instructed me in metabolite profiling and quantifying. Juulia Lautaoja helped me with cell culture and metabolite extractions. I also want to thank my supervisors and mentors for their helpful comments. I also want to thank Heikki Kainulainen and Ulla Sahinaho for their resources and contribution to the BCAA-free pilot experiments. In addition, I want to thank Susanna Luoma, Tanja Toivanen, and Jukka Hintikka for enzyme activity measurements, and Laura Pitkänen and Maarit Hellman for helping in buffer preparation. The data collected in this thesis will be part of a scientific publication and Juulia Lautaoja's doctoral thesis.

REFERENCES

Bekeova C., Anderson-Pullinger L., Boye K., Boos F., Sharpadskaya Y., Herrmann J.M. & Seifert E.L. 2019. Multiple mitochondrial thioesterases have distinct tissue and substrate specificity and CoA regulation, suggesting unique functional roles. *Journal of Biological Chemistry* 294: 19034–19047.

Blomstrand E. & Essén-Gustavsson B. 2009. Changes in amino acid concentration in plasma and type I and type II fibres during resistance exercise and recovery in human subjects. *Amino Acids* 37: 629–636.

Bose S., Ramesh V. & Locasale J.W. 2019. Acetate Metabolism in Physiology, Cancer, and Beyond. *Trends in Cell Biology* 29: 695–703.

Burch N., Arnold A.-S., Item F., Summermatter S., Brochmann Santana Santos G., Christe M., Boutellier U., Toigo M. & Handschin C. 2010. Electric Pulse Stimulation of Cultured Murine Muscle Cells Reproduces Gene Expression Changes of Trained Mouse Muscle. *PLoS ONE* 5: e10970, doi: 10.1371/journal.pone.0010970.

Carter S. & Solomon T.P.J. 2019. In vitro experimental models for examining the skeletal muscle cell biology of exercise: the possibilities, challenges and future developments. *Pflügers Archiv - European Journal of Physiology* 471: 413–429.

Crown S.B., Marze N. & Antoniewicz M.R. 2015. Catabolism of Branched Chain Amino Acids Contributes Significantly to Synthesis of Odd-Chain and Even-Chain Fatty Acids in 3T3-L1 Adipocytes. *PLoS ONE* 10: e0145850, doi: 10.1371/journal.pone.0145850.

Evers-van Gogh I.J.A., Alex S., Stienstra R., Brenkman A.B., Kersten S. & Kalkhoven E. 2015. Electric Pulse Stimulation of Myotubes as an In Vitro Exercise Model: Cell-Mediated and Non-Cell-Mediated Effects. *Scientific Reports* 5: 10944.

Fajardo R.J., Karim L., Calley V.I. & Bouxsein M.L. 2014. A Review of Rodent Models of Type 2 Diabetic Skeletal Fragility. *Journal of Bone and Mineral Research* 29: 1025–1040.

Farmawati A., Kitajima Y., Nedachi T., Sato M., Kanzaki M. & Nagatomi R. 2013. Characterization of contraction-induced IL-6 up-regulation using contractile C2C12 myotubes. *Endocrine Journal*: 137–147.

Furuichi Y., Manabe Y., Takagi M., Aoki M. & Fujii N.L. 2018. Evidence for acute contraction-induced myokine secretion by C2C12 myotubes. *PLoS ONE* 13: e0206146, doi: 10.1371/journal.pone.0206146.

Gibala M.J., MacLean D.A., Graham T.E. & Saltin B. 1998. Tricarboxylic acid cycle intermediate pool size and estimated cycle flux in human muscle during exercise. *American Journal of Physiology-Endocrinology and Metabolism* 275: E235–E242.

Görgens S.W., Hjorth M., Eckardt K., Wichert S., Norheim F., Holen T., Lee S., Langleite T., Birkeland K.I., Stadheim H.K., Kolnes K.J., Tangen D.S., Kolnes A.J., Jensen J., Drevon C.A. & Eckel J. 2016. The exercise-regulated myokine chitinase-3-like protein 1 stimulates human myocyte proliferation. *Acta Physiologica* 216: 330–345.

Görgens S.W., Raschke S., Holven K.B., Jensen J., Eckardt K. & Eckel J. 2013. Regulation of follistatin-like protein 1 expression and secretion in primary human skeletal muscle cells. *Archives of Physiology and Biochemistry* 119: 75–80.

Guimarães-Ferreira L. 2014. Role of the phosphocreatine system on energetic homeostasis in skeletal and cardiac muscles. *Einstein (São Paulo)* 12: 126–131.

Hall G., Sacchetti M. & Rådegran G. 2002. Whole body and leg acetate kinetics at rest, during exercise and recovery in humans. *The Journal of Physiology* 542: 263–272.

Hargreaves M. & Spriet L.L. 2020. Skeletal muscle energy metabolism during exercise. *Nature Metabolism* 2: 817–828.

Hay R. & Bond M. 1967. Kinetics of the Decarboxylation of Acetoacetic acid. *Australian Journal of Chemistry* 20: 1823.

Horibata Y., Ando H., Itoh M. & Sugimoto H. 2013. Enzymatic and transcriptional regulation of the cytoplasmic acetyl-CoA hydrolase ACOT12. *Journal of Lipid Research* 54: 2049–2059.

Horie M., Warabi E., Komine S., Oh S. & Shoda J. 2015. Cytoprotective Role of Nrf2 in Electrical Pulse Stimulated C2C12. *PLoS ONE* 10: e0144835, doi: doi.org/10.1371/journal.pone.0144835.

Hoshino D., Kawata K., Kunida K., Hatano A., Yugi K., Wada T., Fujii M., Sano T., Ito Y., Furuichi Y., Manabe Y., Suzuki Y., Fujii N.L., Soga T. & Kuroda S. 2020. Trans-omic Analysis Reveals ROS-Dependent Pentose Phosphate Pathway Activation after High-Frequency Electrical Stimulation in C2C12 Myotubes. *iScience* 23: 101558.

Hui S., Ghergurovich J.M., Morscher R.J., Jang C., Teng X., Lu W., Esparza L.A., Reya T., Zhan Le, Yanxiang Guo J., White E. & Rabinowitz J.D. 2017. Glucose feeds the TCA cycle via circulating lactate. *Nature* 551: 115–118.

Jakobsdottir G., Bjerregaard J.H., Skovbjerg H. & Nyman M. 2013. Fasting serum concentration of short-chain fatty acids in subjects with microscopic colitis and celiac disease: no difference compared with controls, but between genders. *Scandinavian Journal of Gastroenterology* 48: 696–701.

Kamphorst J.J., Chung M.K., Fan J. & Rabinowitz J.D. 2014. Quantitative analysis of acetyl-CoA production in hypoxic cancer cells reveals substantial contribution from acetate. *Cancer & Metabolism* 2: 23.

Kostidis S., Addie R.D., Morreau H., Mayboroda O.A. & Giera M. 2017. Quantitative NMR analysis of intra- and extracellular metabolism of mammalian cells: A tutorial. *Analytica Chimica Acta* 980: 1–24.

Kujala U.M., Mäkinen V.-P., Heinonen I., Soininen P., Kangas A.J., Leskinen T.H., Rahkila P., Würtz P., Kovanen V., Cheng S., Sipilä S., Hirvensalo M., Telama R., Tammelin T., Savolainen M.J., Pouta A., O'Reilly P.F., Mäntyselkä P., Viikari J., Kähönen M., Lehtimäki T., Elliott P., Vanhala M.J., Raitakari O.T., Järvelin M.-R., Kaprio J., Kainulainen H. & Ala-Korpela M. 2013. Long-term Leisure-time Physical Activity and Serum Metabolome. *Circulation* 127: 340–348.

Legrand C., Bour J.M., Jacob C., Capiaumont J., Martial A., Marc A., Wudtke M., Kretzmer G., Demangel C., Duval D. & Hache J. 1992. Lactate dehydrogenase (LDH) activity of the number of dead cells in the medium of cultured

eukaryotic cells as marker. *Journal of Biotechnology* 25: 231–243.

Lerner A.B. 1949. On the metabolism of phenylalanine and tyrosine. *The Journal of biological chemistry* 181: 281–294.

Lira V.A., Benton C.R., Yan Z. & Bonen A. 2010. PGC-1α regulation by exercise training and its influences on muscle function and insulin sensitivity. *American Journal of Physiology-Endocrinology and Metabolism* 299: E145–E161.

Liu X., Cooper D.E., Cluntun A.A., Warmoes M.O., Zhao S., Reid M.A., Liu J., Lund P.J., Lopes M., Garcia B.A., Wellen K.E., Kirsch D.G. & Locasale J.W. 2018. Acetate Production from Glucose and Coupling to Mitochondrial Metabolism in Mammals. *Cell* 175: 502-513.e13.

Liu X., Xue X., Tian J., Qin X., Zhou S., Chen A. & Han Y. 2021. Skeletal Muscle Metabolomic Responses to Endurance and Resistance Training in Rats under Chronic Unpredictable Mild Stress. *International Journal of Environmental Research and Public Health* 18: 1645.

MacDonald T.L., Pattamaprapanont P., Pathak P., Fernandez N., Freitas E.C., Hafida S., Mitri J., Britton S.L., Koch L.G. & Lessard S.J. 2020. Hyperglycaemia is associated with impaired muscle signalling and aerobic adaptation to exercise. *Nature Metabolism* 2: 902–917.

Martinez D.L., Tsuchiya Y. & Gout I. 2014. Coenzyme A biosynthetic machinery in mammalian cells. *Biochemical Society Transactions* 42: 1112–1117.

MetaMEx. 2020. Meta-analysis of Skeletal Muscle Response to Exercise. https://www.metamex.eu/ , 15.3.2021.

Morville T., Sahl R.E., Moritz T., Helge J.W. & Clemmensen C. 2020. Plasma Metabolome Profiling of Resistance Exercise and Endurance Exercise in Humans. *Cell Reports* 33: 108554.

Nelson D.L. & Cox M.M. 2013. *Lehninger principles of biochemistry*. W. H. Freeman

and Company, New York.

Newman J.C. & Verdin E. 2017. β-Hydroxybutyrate: A Signaling Metabolite. *Annual Review of Nutrition* 37: 51–76.

Newsholme P., Lima M.M.R., Procopio J., Pithon-Curi T.C., Doi S.Q., Bazotte R.B. & Curi R. 2003. Glutamine and glutamate as vital metabolites. *Brazilian Journal of Medical and Biological Research* 36: 153–163.

Nikolić N., Görgens S.W., Thoresen G.H., Aas V., Eckel J. & Eckardt K. 2017. Electrical pulse stimulation of cultured skeletal muscle cells as a model for in vitro exercise - possibilities and limitations. *Acta Physiologica* 220: 310–331.

Nikolić N., Skaret Bakke S., Tranheim Kase E., Rudberg I., Flo Halle I., Rustan A.C., Thoresen G.H. & Aas V. 2012. Electrical Pulse Stimulation of Cultured Human Skeletal Muscle Cells as an In Vitro Model of Exercise. *PLoS ONE* 7: e33203, doi: 10.1371/journal.pone.0033203.

Pan H., Xu X., Hao X. & Chen Y. 2012. Changes of Myogenic Reactive Oxygen Species and Interleukin-6 in Contracting Skeletal Muscle Cells. *Oxidative Medicine and Cellular Longevity* 2012: 1–6.

Pedersen B.K. & Saltin B. 2015. Exercise as medicine - evidence for prescribing exercise as therapy in 26 different chronic diseases. *Scandinavian Journal of Medicine & Science in Sports* 25: 1–72.

Pillon N.J., Gabriel B.M., Dollet L., Smith J.A.B., Sardón Puig L., Botella J., Bishop D.J., Krook A. & Zierath J.R. 2020. Transcriptomic profiling of skeletal muscle adaptations to exercise and inactivity. *Nature Communications* 11: 470.

Powers S.K., Deminice R., Ozdemir M., Yoshihara T., Bomkamp M.P. & Hyatt H. 2020. Exercise-induced oxidative stress: Friend or foe? *Journal of Sport and Health Science* 9: 415–425.

Rabinowitz J.D. & Enerbäck S. 2020. Lactate: the ugly duckling of energy

metabolism. *Nature Metabolism* 2: 566–571.

Raschke S., Eckardt K., Bjørklund Holven K., Jensen J. & Eckel J. 2013. Identification and Validation of Novel Contraction-Regulated Myokines Released from Primary Human Skeletal Muscle Cells. *PLoS ONE* 8: e62008, doi: 10.1371/journal.pone.0062008.

Schranner D., Kastenmüller G., Schönfelder M., Römisch-Margl W. & Wackerhage H. 2020. Metabolite Concentration Changes in Humans After a Bout of Exercise: a Systematic Review of Exercise Metabolomics Studies. *Sports Medicine - Open* 6: 11.

Shimomura Y., Murakami T., Nakai N., Nagasaki M. & Harris R.A. 2004. Exercise Promotes BCAA Catabolism: Effects of BCAA Supplementation on Skeletal Muscle during Exercise. *The Journal of Nutrition* 134: 1583S-1587S.

Su X., Magkos F., Zhou D., Eagon J.C., Fabbrini E., Okunade A.L. & Klein S. 2015. Adipose tissue monomethyl branched-chain fatty acids and insulin sensitivity: Effects of obesity and weight loss. *Obesity* 23: 329–334.

Svensson K., Albert V., Cardel B., Salatino S. & Handschin C. 2016. Skeletal muscle PGC-1α modulates systemic ketone body homeostasis and ameliorates diabetic hyperketonemia in mice. *The FASEB Journal* 30: 1976–1986.

Tillander V., Arvidsson Nordström E., Reilly J., Strozyk M., Veldhoven P.P. Van, Hunt M.C. & Alexson S.E.H. 2014. Acyl-CoA thioesterase 9 (ACOT9) in mouse may provide a novel link between fatty acid and amino acid metabolism in mitochondria. *Cellular and Molecular Life Sciences* 71: 933–948.

Vysochan A., Sengupta A., Weljie A.M., Alwine J.C. & Yu Y. 2017. ACSS2-mediated acetyl-CoA synthesis from acetate is necessary for human cytomegalovirus infection. *Proceedings of the National Academy of Sciences* 114: E1528–E1535.

Wallace M., Green C.R., Roberts L.S., Lee Y.M., McCarville J.L., Sanchez-

Gurmaches J., Meurs N., Gengatharan J.M., Hover J.D., Phillips S.A., Ciaraldi T.P., Guertin D.A., Cabrales P., Ayres J.S., Nomura D.K., Loomba R. & Metallo C.M. 2018. Enzyme promiscuity drives branched-chain fatty acid synthesis in adipose tissues. *Nature Chemical Biology* 14: 1021–1031.

Zhang J., Bhattacharyya S., Hickner R.C., Light A.R., Lambert C.J., Gale B.K., Fiehn O. & Adams S.H. 2019. Skeletal muscle interstitial fluid metabolomics at rest and associated with an exercise bout: application in rats and humans. *American Journal of Physiology-Endocrinology and Metabolism* 316: E43–E53.

Zhou L., Wang L., Lu L., Jiang P., Sun H. & Wang H. 2012. Inhibition of miR-29 by TGF-beta-Smad3 Signaling through Dual Mechanisms Promotes Transdifferentiation of Mouse Myoblasts into Myofibroblasts. *PLoS ONE* 7: e33766, doi: 10.1371/journal.pone.0033766.

APPENDIX 1. Acquisition and processing parameters of the two-dimensional NMR experiments and spectra

Acquisition parameter	**$^{1}H-^{13}C$ HSQC**	**$^{1}H-^{13}C$ HSQC-TOCSY**	**$^{1}H-^{1}H$ TOCSY**	**$^{1}H-^{1}H$ DQF-COSY**
Number of scans	64	256	32	16
Complex points of FID(F2, F1)	1024, 128	1024, 128	2050, 256	1024, 256
Spectral width (ppm, F2, F1)	16.0192, 165.00	16.0192, 164.9856	13.9452, 13.9452	10.9991, 11.0000
Acquisition time (s, F1, F2)	0.0799, 0.00385	0.0799, 0.003855	0.1836800, 0.0229376	0.1163264, 0.0290791
Receiver gain	128	203	203	128
Dwell time (μs)	39.0	39.0	44.8	56.9
Digital resolution	22	22	22	22
Processing parameter	**$^{1}H-^{13}C$ HSQC**	**$^{1}H-^{13}C$ HSQC-TOCSY**	**$^{1}H-^{1}H$ TOCSY**	**$^{1}H-^{1}H$ DQF-COSY**
Size of real spectrum (F2, F1)	4096, 1024	4096, 1024	4096, 4096	4096, 2048
Window function	QSINE	QSINE	QSINE	QSINE
Sine bell shift (F2, F1)	2, 2	2, 2	2, 2	2, 2
Linear prediction (F1)	Forward, complex (LPfc)	Forward, complex (LPfc)	Forward, complex (LPfc)	Forward, complex (LPfc)

APPENDIX 2. The used driver peaks for the quantification

	Medium extracts	Cell extracts
Compound	**The "driver peak" that was used for quantification (σ ^{1}H, ppm)**	**The "driver peak" that was used for quantification (σ ^{1}H, ppm)**
ADP		8.53
3-Hydroxybutyrate	1.19	
2-Methylbutyrate (Using butyrate function)	0.85	0.85
Acetate	1.91	1.91
Alanine	1.47	1.47
Arginine	3.24	3.24
Asparagine	2.87	
Aspartate		2.80
Choline	3.20	
Citrate	2.52	2.65
Creatine	3.92	3.027
Phosphocreatine		3.033
Cystine	3.19	
Ethanol	1.17	
Formate	8.45	8.45
Fumarate	6.51	6.51
Glucose	3.54	3.24
Glutamate	2.35	2.35
Glutamine	2.47	2.46
Glycine	3.56	3.55
Guanidoacetate		3.78
Histidine	7.09	
Isobutyrate	1.05	1.05
Isoleucine	1.00	1.00
Isovalerate	0.90	0.90
Lactate	1.32	1.32
Leucine	0.96	0.96
Lysine	3.02	3.02
Malate		2.66
Methanol	3.35	3.34
myo-Inositol	3.62	3.53
NAD+		6.03
Niacinamide	8.25	7.59
Nicotinate	8.25	
O-Phosphocholine		3.21
Pantothenate		0.89
Phenylalanine	7.42	7.42
Propionate		1.04
Pyridoxine	2.46	
Pyroglutamate	4.17	
Serine	0.42	
sn-Glycero-3-phosphocholine		3.22
Succinate	2.39	2.39
Taurine		3.26
Threonine	1.32	1.32
Tryptophan	7.54	
Tyrosine	7.19	6.89
UDP-glucose		5.60
Valine	1.03	1.03
β-Alanine		3.17

APPENDIX 3. Spike-in experiments of isobutyrate, isovalerate, and niacinamide

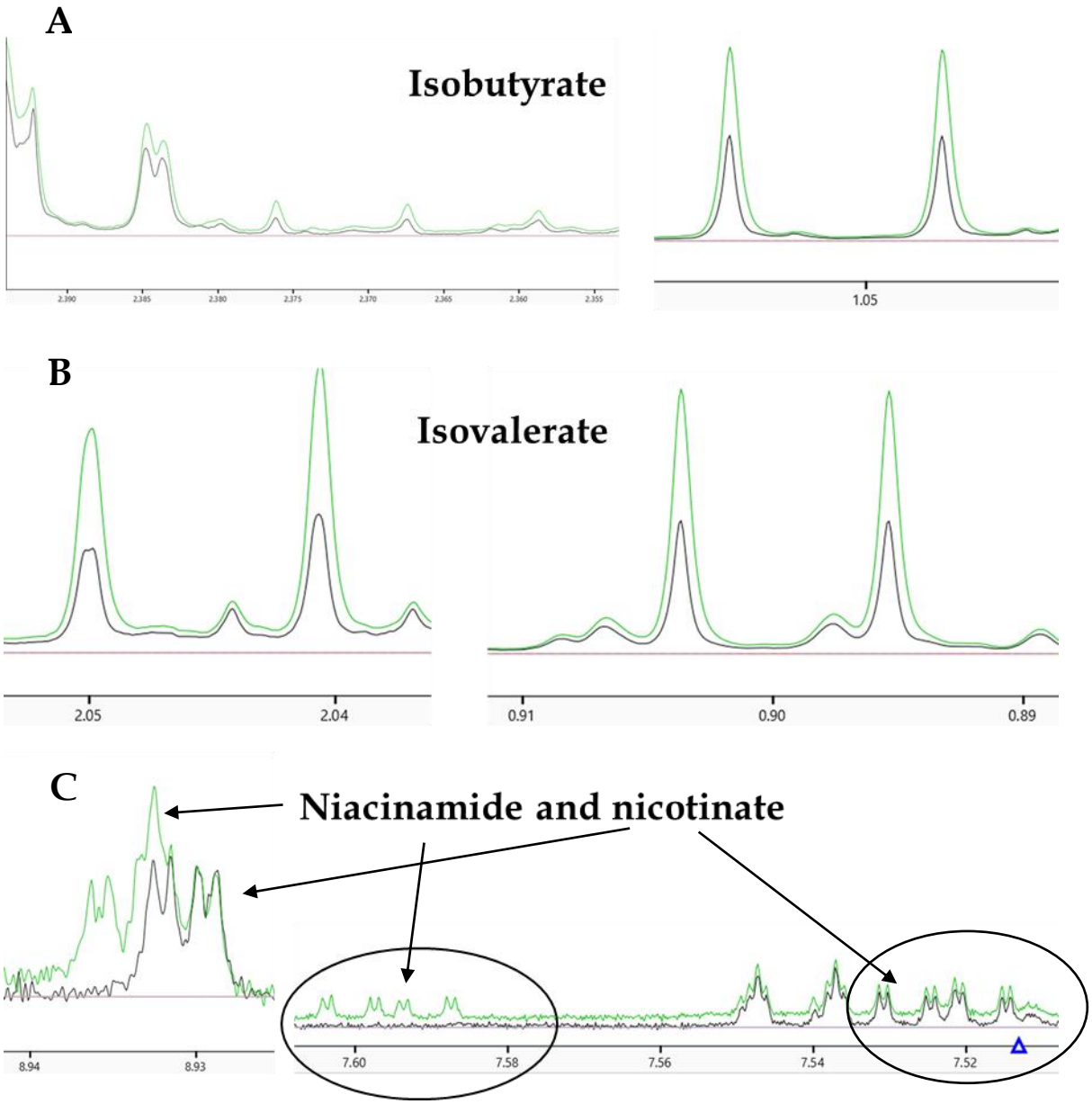

Identification of the Isobutyrate, isovalerate, niacinamide, and nicotinate was confirmed by spike-in experiments. 1H NMR spectrum was recorded before (black spectrum) and after (green spectrum) adding commercial isobutyrate/isovalerate/niacinamide into one of the samples. (A) The spike-in experiment of isobutyrate. One can see that the candidate peaks increased after addition. (B) The spike-in experiment of isovalerate. One can see that the candidate peaks increased after addition. (C) Spike-in experiment of niacinamide/nicotinate. The peaks of the black spectrum were candidate peaks of nicotinate. Green spectrum was recorded after the addition of the niacinamide. This experiment confirmed that niacinamide was converted into nicotinate in 12 of 14 EPS samples.

APPENDIX 4. Content of the high and low glucose Dulbecco´s modified eagle medium (DMEM, #BE12-614F and #BE12-707F, respectively, Lonza, Basel, Switzerland).

	High Glucose	Low Glucose
Amino acids	**mM**	**mM**
L-arginine hydrochloride	0.4	0.4
L-cystine	0.2	0.2
Glycine	0.4	0.4
L-histidine	0.2	0.2
L-isoleucine	0.8	0.8
L-leucine	0.8	0.8
L-lysine hydrochloride	0.8	0.8
L-methionine	0.2	0.2
L-phenylalanine	0.4	0.4
L-serine	0.4	0.4
L-threonine	0.8	0.8
L-tryptophan	0.1	0.1
L-tyrosine	0.4	0.4
L-valine	0.8	0.8
Vitamins	**mM**	**mM**
Choline chloride	0.03	0.03
D-calcium pantothenate	0.01	0.01
Folic acid	0.01	0.01
Nicotinamide	0.03	0.03
Pyrodoxal hydrochloride	0.02	0.02
Riboflavin	0.001	0.001
Thiamine hydrochloride	0.01	0.01
I-inositol	0.04	0.04
Inorganic salts	**mM**	**mM**
Calcium chloride	1.8	1.8
Ferric nitrate nonhydrate	0.00025	0.00025
Magnesium sulfate	0.8	0.8
Potassium chloride	5.4	5.4
Sodium bicarbonate	44	44
Sodium chloride	109.5	109.5
Sodium phosphate monobasic	0.9	0.9
Other components	**mM**	**mM**
D-glucose	25.0	5.55
Phenol red	0.04	0.04
Pyruvic acid sodium salt	1	1

APPENDIX 5. ^{1}H and ^{1}H – ^{1}H TOCSY spectra of 3-hydroxybutyrate

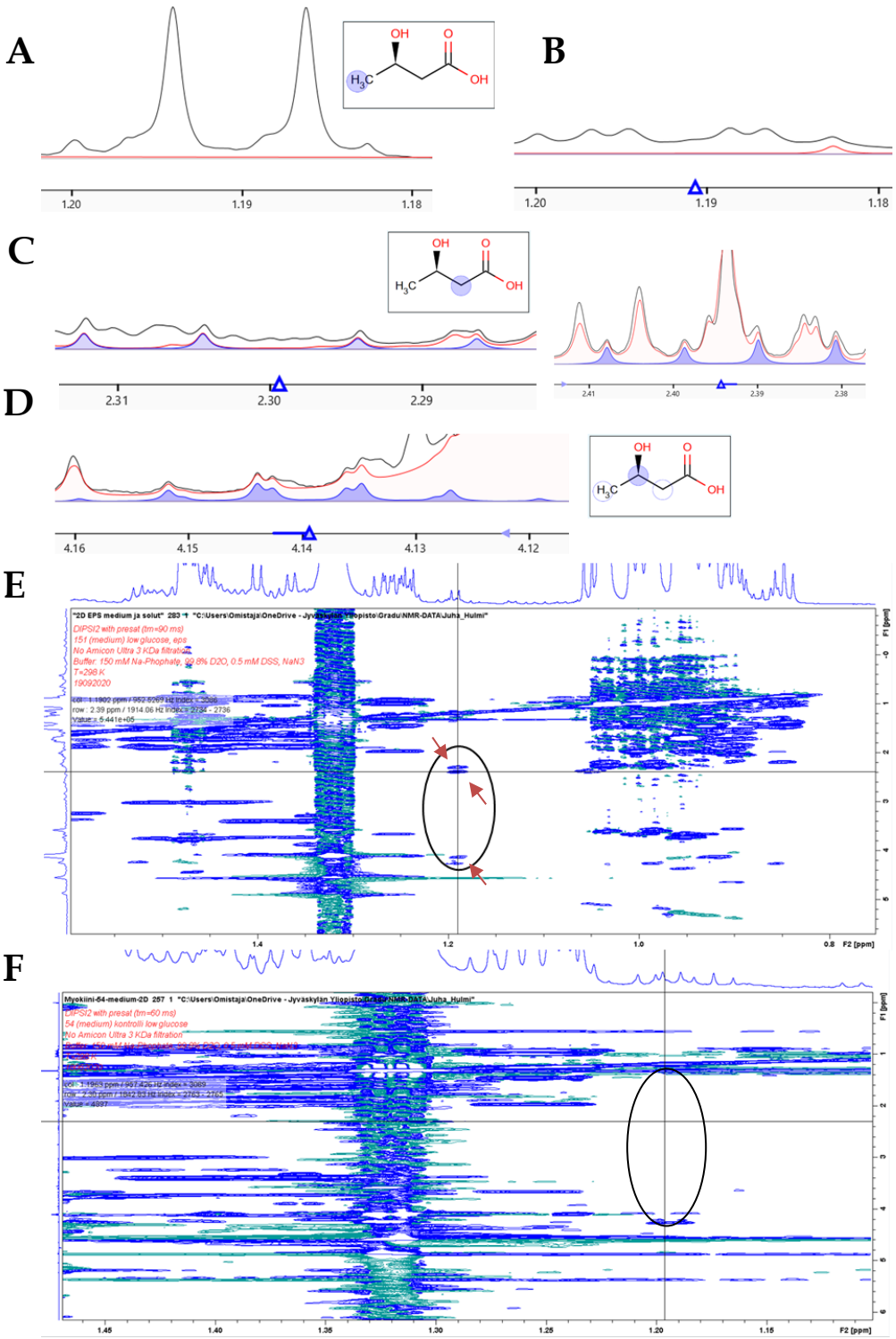

(A) The methyl peak (a doublet) of 3-hydroxybutyrate of an EPS sample. (B) Some background peaks of an unknown compound of a fresh medium sample. (C) Quartets of the α-hydrogen of the 3-hydroxybutyrate and their Chenomx fits. (D) Signal of the β-hydrogen and its fit in Chenomx. (E) ^{1}H – ^{1}H TOCSY spectrum of the EPS sample. One can see that the methyl protons are coupled with the three other signals. (F) ^{1}H – ^{1}H TOCSY spectrum of a non-EPS sample

from where one can see that there are no couplings (cross-peaks) with the putative methyl signal.

APPENDIX 6. Spearman's correlation coefficients between branched short-chain fatty acids and branched-chain amino acids in cell extracts and the medium samples

Cells

Correlations

			Isoleucine	2-methylbutyrate	Isobutyrate	Isovalerate	Leucine	Valine
Spearman's rho	Isoleucine	Correlation Coefficient	1,000	,784**	,827**	,859**	,973**	,994**
		Sig. (2-tailed)	.	,000	,000	,000	,000	,000
		N	26	26	26	26	26	26
	2-methylbutyrate	Correlation Coefficient	,784**	1,000	,942**	,947**	,807**	,812**
		Sig. (2-tailed)	,000	.	,000	,000	,000	,000
		N	26	26	26	26	26	26
	Isobutyrate	Correlation Coefficient	,827**	,942**	1,000	,955**	,863**	,854**
		Sig. (2-tailed)	,000	,000	.	,000	,000	,000
		N	26	26	26	26	26	26
	Isovalerate	Correlation Coefficient	,859**	,947**	,955**	1,000	,898**	,887**
		Sig. (2-tailed)	,000	,000	,000	.	,000	,000
		N	26	26	26	26	26	26
	Leucine	Correlation Coefficient	,973**	,807**	,863**	,898**	1,000	,987**
		Sig. (2-tailed)	,000	,000	,000	,000	.	,000
		N	26	26	26	26	26	26
	Valine	Correlation Coefficient	,994**	,812**	,854**	,887**	,987**	1,000
		Sig. (2-tailed)	,000	,000	,000	,000	,000	.
		N	26	26	26	26	26	26

**. Correlation is significant at the 0.01 level (2-tailed).

Medium

Correlations

			2-methylbutyrate	Isobutyrate	Isovalerate	Isoleucine	Leucine	Valine
Spearman's rho	2-methylbutyrate	Correlation Coefficient	1,000	,526**	,464*	-,007	-,234	-,086
		Sig. (2-tailed)	.	,004	,013	,971	,230	,662
		N	28	28	28	28	28	28
	Isobutyrate	Correlation Coefficient	,526**	1,000	,777**	,011	-,177	,005
		Sig. (2-tailed)	,004	.	,000	,957	,367	,978
		N	28	28	28	28	28	28
	Isovalerate	Correlation Coefficient	,464*	,777**	1,000	,199	,003	,162
		Sig. (2-tailed)	,013	,000	.	,311	,988	,410
		N	28	28	28	28	28	28
	Isoleucine	Correlation Coefficient	-,007	,011	,199	1,000	,714**	,875**
		Sig. (2-tailed)	,971	,957	,311	.	,000	,000
		N	28	28	28	28	28	28
	Leucine	Correlation Coefficient	-,234	-,177	,003	,714**	1,000	,870**
		Sig. (2-tailed)	,230	,367	,988	,000	.	,000
		N	28	28	28	28	28	28
	Valine	Correlation Coefficient	-,086	,005	,162	,875**	,870**	1,000
		Sig. (2-tailed)	,662	,978	,410	,000	,000	.
		N	28	28	28	28	28	28

**. Correlation is significant at the 0.01 level (2-tailed).

*. Correlation is significant at the 0.05 level (2-tailed).